ISSN 1849–0751 (On–line)
ISSN 0013–7448 (Print)
UDK 621.31
https://doi.org/10.37798/EN2024734

Journal of Energy

VOLUME 73 Number 4 | 2024

ENERGIJA 73

Journal of Energy

Scientific Professional Journal Of Energy, Electricity, Power Systems
Online ISSN 1849–0751, Print ISSN 0013–7448, VOL 73
https://doi.org/10.37798/EN2024734

Published by
HEP d.d., Ulica grada Vukovara 37, HR–10000 Zagreb
HRO CIGRÉ, Berislavićeva 6, HR–10000 Zagreb

EDITORIAL

In the paper "PV Integration in LV Networks and Capacity Analysis" the authors address one of the key technical challenges of the energy transition: the integration of photovoltaic (PV) systems into low-voltage (LV) distribution networks. The paper presents a detailed simulation-based analysis using MATLAB to model voltage drops and conductor capacities for varying PV penetration levels—from 3 kW to 8 kW per consumer. A significant innovation lies in the use of a feedforward neural network trained on solar irradiance, temperature, and cloud cover to forecast day-ahead PV generation. The results confirm that the LV network can safely host up to 8 kW of PV per household without violating voltage limits (+5%, -10%) or exceeding conductor thermal thresholds. The comparison between modeled and predicted generation shows minimal deviation, validating the proposed predictive framework. The study underlines the importance of combining accurate forecasting with iterative capacity evaluation to support reliable and optimized renewable integration in residential networks.

The second paper, "Diesel Engine Performance and Emission Properties using Kariya Biodiesel" evaluates diesel engine performance and emission properties when fuelled with an already-produced kariya oil biodiesel (KOB) and KOB blends. The performance evaluation (fuel consumption, brake power, and exhaust gas temperature) of a diesel engine (Nulux R175A Diesel Engine) fuelled with KOB and its blends were determined. The brake power and the exhaust gas temperature were determined during operation using a Schenck W230 Eddy Current dynamometer and a thermometer respectively. Using a hand-held exhaust gas analyzer (Product Model: Aeroqual Series 500), emission characteristics were also determined. It was observed that the fuel consumed by the engine increased as biodiesel increased in the blends. Importantly, the study confirms that KOB has favorable combustion characteristics and can serve as a sustainable biofuel option without competing with food production.

The third paper, "The Roles of Battery Energy Storage System in Different Energy Communities" examines the role of Battery Energy Storage Systems in three distinct types of energy communities: self-consumption-oriented, prosumer-sharing, and grid-supporting. Using simulations based on real consumption and generation data, the authors explore how BESS sizing and control strategies affect key performance indicators such as self-sufficiency, grid exchange, and energy balancing. The findings show that a well-dimensioned BESS can increase local energy self-consumption by over 60% and reduce grid dependency significantly during peak hours. In community-sharing configurations, storage enables energy sharing between households with asynchronous demand and production patterns. The study also emphasizes that the optimal operation of BESS depends on regulatory support and appropriate business models that incentivize storage investment and participation in flexibility markets.

The article "Regional Solar Irradiance Forecasting Using Multi-Camera Sky Imagery and Machine Learning Models" presents a cutting-edge approach to short-term solar irradiance forecasting using machine learning and sky imagery from multiple ground-based cameras. The authors implement a convolutional neural network (CNN) trained on images of sky conditions and concurrent meteorological parameters to predict solar radiation over a short time horizon. By comparing model outputs with measured irradiance data, the CNN-based method demonstrated high accuracy, especially in detecting fast-moving cloud cover changes that traditional numerical weather prediction models often miss. The proposed method is computationally efficient and highly scalable, making it suitable for regional PV plant operation and grid dispatch planning. This work represents a significant advancement in solar forecasting techniques, offering a valuable tool for managing variability in solar energy generation.

Igor Kuzle
Editor–in–Chief

Journal of Energy

VOLUME 73 Number 4 | 2024

journal homepage: http://journalofenergy.com/

PV Integration in LV Networks and Capacity Analysis

Maja Muftić Dedović, Samir Avdaković, Adin Memić

***Summary* — The increasing integration of photovoltaic (PV) systems in low-voltage (LV) networks presents challenges in violation of permitted voltage changes in the LV network and conductor and transformer capacity, which are critical for maintaining grid reliability and operational efficiency. This paper analyzes PV integration, focusing on voltage control, conductor capacity, and the importance of day-ahead PV generation and consumption for proactive grid management. Using MATLAB, the LV network is modeled to assess voltage analysis and conductor capacity for PV capacities ranging from 3 kW to 8 kW per consumer. Predictions of day-ahead PV production are conducted using a feedforward neural network trained on meteorological data such as solar irradiance, temperature, and cloud cover. The predictive model enabled voltage drop simulations and capacity analysis under forecasted conditions. The results demonstrated that voltage levels remained within the permissible range (+5%, -10% of 400 V) for PV capacities up to 8 kW, ensuring operational reliability. The neural network-based predictions are closely aligned with modeled values, with minimal differences, validating the forecasting approach. Voltage variations increased with higher PV capacities, but conductor current levels consistently remained below thermal limits. Incremental PV capacity integration revealed the network's ability to support distributed generation effectively but with limitations at higher capacities. This research highlights the role of accurate forecasting and optimization in ensuring reliable renewable energy adoption.**

***Keywords* — Distributed Energy Resources (DERs), Low-Voltage Networks, Neural Networks, Optimization, Prosumers, Voltage Analysis.**

I. Introduction

The increasing penetration of distributed energy resources (DERs), particularly photovoltaic (PV) systems, poses significant challenges and opportunities for modern power distribution networks. With the emergence of prosumers, entities capable of both consuming and producing electricity, and energy communities, the dynamics of energy generation, consumption, and grid interaction are rapidly evolving. Efficiently managing these interactions is critical to ensuring grid stability, optimizing energy utilization, and supporting the transition towards sustainable energy systems.

(Corresponding author: Maja Muftić Dedović)

Maja Muftić Dedović, Samir Avdaković, and Adin Memić are with the Faculty of Electrical Engineering, University of Sarajevo, Sarajevo, Bosnia and Herzegovina (e-mails: maja.muftic-dedovic@etf.unsa.ba, samir.avdakovic@etf.unsa.ba, adin.memic@etf.unsa.ba)

Reference [1] address these challenges by proposing a distributed congestion management scheme based on iterative distribution locational marginal pricing (iDLMP). Their approach optimizes prosumer energy operations to alleviate congestion in distribution networks. By considering prosumers as self-organizing units capable of integrating diverse resource flexibilities their scheme enhances local energy sharing and supports the efficient integration of DERs. Incorporating such innovative congestion management strategies is crucial for improving hosting capacities and ensuring stable operation of low-voltage (LV) networks with high DER penetration. Building upon these insights, this research aims to further optimize prosumer integration by addressing voltage regulation challenges and conductor capacity evaluation.

One of the primary challenges associated with PV integration is managing the voltage variations caused by fluctuating energy generation. These fluctuations can lead to voltage drops or rise, potentially exceeding permissible limits and impacting the quality of the power supply. Additionally, the capacity of existing conductors may be insufficient to handle the increased power flow, necessitating careful evaluation to avoid thermal overloads and maintain operational safety.

This paper addresses these challenges by analyzing the effects of PV integration on voltage profiles and conductor capacity in LV networks. The research employs a systematic methodology to evaluate the feasibility of PV integration while ensuring network reliability and compliance with operational standards. The proposed approach includes modeling the network's electrical and geometric characteristics, assessing PV production dynamics, and conducting iterative optimization to identify maximum permissible PV capacities.

The findings of this research aim to provide practical insights for grid operators, policymakers, and engineers in planning and optimizing PV system integration in LV networks, ensuring a balance between renewable energy adoption and system reliability.

A key novelty of this paper is the quantitative evaluation of PV hosting capacity under different penetration scenarios while ensuring compliance with operational voltage limits and conductor thermal ratings. The paper also introduces an iterative assessment methodology that systematically determines the maximum allowable PV capacity in an LV network, offering valuable insights for grid operators and planners.

The comparative analysis of modeled against forecasted PV production demonstrates the reliability of predictive approaches in assessing voltage within permissible limits, reinforcing the importance of proactive grid management. The findings contribute to a more precise estimation of hosting capacity, ensuring efficient integration of renewable energy sources without compromising network reliability.

Maja Muftić Dedović, Samir Avdaković, Adin Memić, PV Integration in LV Networks and Capacity Analysis, Journal of Energy, vol. 73 Number 4 (2024), 3–11
https://doi.org/10.37798/2024734698

The key contributions of this paper are as follows.

1. The paper provides a quantitative evaluation of PV hosting capacity in LV networks while ensuring compliance with operational voltage limits and conductor thermal ratings.
2. An iterative assessment methodology is introduced to determine the maximum allowable PV penetration under different scenarios, offering practical insights for grid operators and planners.
3. The research validates the accuracy of predictive models by comparing modeled and forecasted PV generation, ensuring that voltage levels remain within permissible limits.
4. Realistic daily and seasonal load variations are considered, acknowledging their impact on PV integration and network performance.
5. The findings highlight the importance of predictive approaches in optimizing PV integration, facilitating better planning and operational decision-making for LV networks.

This paper is structured as follows. Section II provides a review of relevant literature, highlighting existing research on PV integration in LV networks and identifying key gaps addressed in this research. Section III describes the proposed methodology, including network modeling, PV generation characteristics, and the iterative assessment approach used for hosting capacity evaluation. Section IV presents the implementation of day-ahead PV output prediction using a neural network model, supporting capacity analysis under forecasted conditions. Section V discusses the results obtained from simulations, comparing modeled and forecasted PV production and analyzing voltage and conductor constraints. Finally, Section VI concludes the paper by summarizing key findings and outlining potential directions for future research.

II. Literature Review

Recent advancements in integrating prosumers into power systems emphasize the critical role of digitalization and advanced optimization techniques. Paper [2] explore the strategic behavior of prosumers in electricity markets, demonstrating how DER investments are influenced by market dynamics and proposing regulatory measures to align private and public incentives. Also, [3] introduces a decentralized Virtual Aggregation Environment (VAE), enabling smart prosumers to collaboratively manage flexibility without a central aggregator, highlighting the potential of cooperative-competitive algorithms for enhancing grid reliability. In [4] is employed multi-agent reinforcement learning (MARL) to optimize peer-to-peer energy trading, showing how dynamic pricing mechanisms can improve community self-sufficiency and reduce costs while balancing local supply and demand.

An Internet of Energy (IoE) framework facilitates bidirectional energy transactions and integrates DERs into virtual power plants, with optimization techniques playing a key role in enhancing grid reliability [5]. A stochastic bottom-up model analyzes the effects of PV self-consumption on load profiles, emphasizing the need for detailed prosumer-level modeling to improve forecasting and grid planning [6]. A prosumer-centric peer-to-peer energy trading approach addresses network voltage constraints, balancing social welfare with economic and technical objectives in energy markets [7].

In [8], a hybrid control policy is proposed to address locational disparities in voltage regulation and economic arbitrage, enhancing grid stability and prosumer benefits. The research in [9] focuses on optimizing DER under uncertainty through improved risk management in decision-making models. The research in [10] examines the impact of distribution tariffs on prosumer demand response, highlighting trade-offs between energy costs and distribution expenses. An incentive-based voltage regulation framework for unbalanced radial networks is developed in [11], balancing prosumer participation and grid needs while reducing operational costs. In [12], an innovative energy management system for LV networks is presented, utilizing prosumer-based ancillary services to manage voltage and reduce congestion.

Challenges such as reverse power flows and voltage fluctuations in LV grids, caused by high penetration of DERs, require advanced grid management tools to improve hosting capacities and maintain stability [13]. A probabilistic approach for maximizing PV hosting capacity through the coordinated management of OLTCs, PV inverters, and EVs demonstrates significant potential for enhancing grid performance and stability [14].

In [15], Prosumer Energy Management Systems (PEMS) are developed to highlight prosumers' dual role as consumers and producers, focusing on advanced communication and optimization techniques for energy sharing and smart grid operations. The research in [16] presents a transactive energy framework using coordinated power control and game theory to optimize prosumer participation, addressing economic incentives and voltage stability. In [17], the financial viability of photovoltaic-battery systems (PV-BSS) is examined, exploring the role of demand response and capacity markets, while identifying challenges related to uncertainty and limited policy support. Reference [18] analyzes the hosting capacity of residential grids with high PV penetration and distributed storage, demonstrating how advanced management systems and coordinated storage utilization mitigate voltage instability and enhance capacity. Finally, [19] reassesses voltage variation strategies, emphasizing that while effective in certain conditions, traditional methods face limitations in achieving substantial energy savings in advanced systems.

Paper [20] explores the role of energy prosumers in sustainable energy transitions, highlighting the socio-economic and policy dimensions of prosumer-driven systems. They underline the need for decentralized configurations and innovative business models to maximize prosumer contributions to net-zero targets. Research in [21] explores energy storage systems (ESS) for active power management and voltage regulation, proposing strategies to maintain grid stability while enhancing prosumer benefits. Also, [22] addresses challenges such as overvoltage and reverse power flow in residential grids with high PV penetration, suggesting scalable battery systems and solar radiation forecasting to ensure voltage stability and energy quality.

Recent research highlights the need to shift from deterministic to stochastic methods for hosting capacity (HC) estimation. Deterministic approaches, though simpler, often overlook the complexities of variable renewable generation and load uncertainties. Stochastic models, such as those in [23], incorporate these uncertainties using advanced optimization techniques, improving accuracy and efficiency over traditional methods. Similarly, [24] demonstrates the limitations of deterministic frameworks and validates the advantages of stochastic approaches in managing PV penetration. Further advancements in HC, as discussed in [25], focus on ESS and dynamic hosting capacity (DHC) strategies, which address voltage rise and reverse power flow issues while enhancing grid reliability through adaptive control and storage integration.

Previous researches on PV hosting capacity have primarily focused on deterministic methods that evaluate network constraints under fixed operating conditions. Unlike these researches, this paper presents a comprehensive approach that integrates both voltage regulation and conductor thermal constraints while systematically determining the maximum feasible PV penetration using an iterative evaluation method. In addition, a comparative analysis

Maja Muftić Dedović, Samir Avdaković, Adin Memić, PV Integration in LV Networks and Capacity Analysis, Journal of Energy, vol. 73 Number 4 (2024), 3–11
https://doi.org/10.37798/2024734698

between modeled and forecasted PV generation ensures that the methodology aligns with real-world operational conditions.

III. METODOLOGY

This paper explores the effects of integrating PV systems into LV distribution networks, emphasizing voltage analysis and conductor capacity evaluation. The proposed methodology provides a systematic approach for assessing the feasibility of PV integration while maintaining network reliability. In Figure 1, the algorithm is presented as a flowchart illustrating the applied approach.

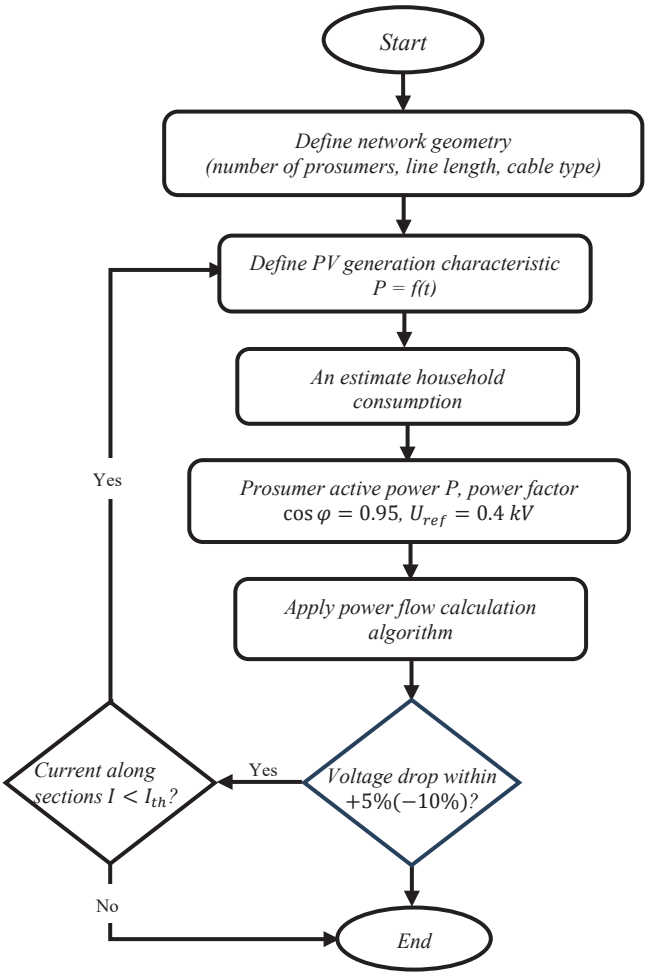

Fig. 1. Flowchart of the applied approach.

A. Network Definition

The geometry of the LV network is characterized by defining the number of consumers or prosumers, the length of distribution lines, and the type of cables used. The length of the cables and their material properties directly influence the resistance and impedance, which are crucial for calculating voltage variations and power losses.

The LV distribution network in this research is modeled with a focus on its electrical and geometric characteristics, including conductor specifications, supply network parameters, transformer details, and load distribution.

The LV network utilizes XP00-A type conductors with a cross-sectional area of 4×70 mm². The electrical characteristics of these conductors include a phase resistance of 0.443 Ω/km, a phase reactance of 0.075 Ω/km, a zero-sequence resistance of 1.772 Ω/km, and a zero-sequence reactance of 0.225 Ω/km. The continuous current-carrying capacity of the conductors is 192A. These parameters directly influence the impedance of the network and, consequently, the voltage profile and power losses.

The LV network is fed by a medium-voltage (MV) network operating at a nominal voltage of 10 kV, with a short-circuit power of 250 MVA and an impedance ratio (R/X) of 0.1. The transformer linking the MV and LV networks is rated at 160 kVA and operates with a primary voltage of 10 kV and a secondary voltage of 0.4 kV. Its short-circuit voltage is 4%, and its copper and iron losses are 2.35 kW and 0.46 kW, respectively. The no-load current is 2.3 A, with impedance ratios (Ro/Rt) of 2.0 and (Xo/Xt) of 1.0.

The LV network's nominal voltage is 0.4 kV, with a permissible voltage limit of +5% (-10%) under normal operation conditions. The network primarily serves residential consumers. The diversity factor for a large number of households is set at 0.17, and the typical power factor is 0.95. These parameters represent a realistic load profile for residential areas. A total of 10 consumers are observed on one segment of the low-voltage distribution (cable).

The network's design includes evenly distributed nodes along the outgoing feeder, with specific distances between them. The distances between successive nodes vary, including segments of 0.05 km, 0.025 km, and 0.075 km. These variations reflect the actual spatial distribution of connections in residential neighborhoods and are crucial for calculation of voltage changes and current flows. The cumulative impedance of the network is determined by summing the impedance contributions of these individual segments. This arrangement ensures an accurate representation of real-world network conditions, enabling precise modeling and analysis of voltage profiles and conductor utilization.

B. Defining PV Characteristics

The production of PV is modeled as a time-dependent function, P=f(t), which accounts for the variation in solar irradiance throughout the day. This function includes factors such as the geographical location, orientation of the panels, and meteorological conditions, all of which impact the energy output of the PV system. A time-series simulation is employed to capture daily and seasonal fluctuations in PV generation, ensuring accurate modeling of the system's behavior.

In addition to PV generation variability, household electricity consumption exhibits daily and seasonal fluctuations, which can influence voltage profiles and network constraints. Higher electricity demand during peak evening hours or winter months may lead to increased voltage drops and higher conductor loading, potentially affecting the network's ability to accommodate additional PV capacity. Conversely, lower demand during midday hours, when PV generation is at its peak, may contribute to higher voltage rise, especially in low-load scenarios.

To ensure a realistic assessment of PV hosting capacity, the methodology considers representative daily load profiles. However, incorporating stochastic load modeling in future research could provide a more detailed evaluation of how dynamic consumption patterns interact with PV generation, allowing for more accurate grid planning and adaptive voltage regulation strategies.

The analysis of electricity production from PV systems is conducted for installed capacities ranging from 3 kW to 8 kW in increments of 1 kW. The simulation is performed using a mathematical model that tracks changes in solar radiation intensity throughout the day, taking into account local climatic and geographical conditions characteristic of regions with a temperate climate. Ideal conditions for a clear day are simulated, with solar radiation intensity peaking at midday. It is assumed that the

Maja Muftić Dedović, Samir Avdaković, Adin Memić, PV Integration in LV Networks and Capacity Analysis, Journal of Energy, vol. 73 Number 4 (2024), 3–11
https://doi.org/10.37798/2024734698

panels are installed on a roof with an optimal orientation. These parameters enabled the creation of a daily production profile that follows a typical solar radiation curve.

For a PV system with a capacity of 6 kW, the electricity production over 24 hours, expressed in kilowatts (kW), is shown in Figure 2.b). The production and consumption refer to June 21st, the longest day of the year, also known as the summer solstice.

For higher-capacity systems, such as an 8 kW system, the production curve retains a similar daily pattern, but peak values are proportionally higher. The simulation is carried out under standard test conditions with a maximum irradiance of 1000 W/m² and a panel temperature of 25°C. The production values are validated by comparison with reference data from the literature and standardized simulations for PV systems in similar climatic regions [26,27].

Figure 2. presents the hourly variation of electricity consumption, PV production, and net power demand over a 24-hour for a 6 kW PV system per consumer.

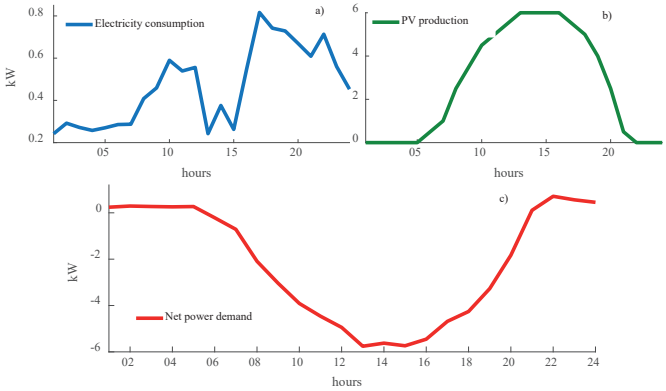

Fig. 2. a.) Electricity consumption, b.) PV Production, and c.) Net power demand over 24 hours for 6 kW.

C. Calculation of Power Demand

For the analysis, household electricity consumption data is calculated over a 24-hour period. The estimated load curve for the year 2024, sourced from the official documents of Public Enterprise Electric Utility of Bosnia and Herzegovina [28], is used as the basis. This curve is multiplied by the average monthly electricity consumption per household in Bosnia and Herzegovina, which is approximately 325 kWh (for June) [29]. The average monthly consumption is calculated by dividing the annual consumption by 12, providing a representative value for analysis. The data is calculated hourly, with each entry representing the average power consumption in kW during one hour. The collected data reflects the dynamics of daily consumption, including variations caused by daily activities, the use of household appliances, and external factors such as temperature and user habits. The collected data is visualized through time series (Figure 2.b)), illustrating changes in consumption throughout the day and enabling the identification of peak loads and periods of reduced consumption.

The net power demand of households (P_D) is determined by subtracting the power supplied by PV panels (P_{PV}) from the household's total power requirements (P_{total}). This relationship is expressed as:

$$P_D = P_{total} - P_{PV}. \quad (1)$$

where:

P_D: The net power demand from the distribution network,

P_{total}: The household's internal power demand,

P_{PV}: The power generated by the PV system.

Negative values in the calculated power demand (Figure 2.c)) and Figure 3.) indicate instances where the PV system produced more energy than the household consumption, potentially leading to energy export or storage opportunities. This net power demand is subsequently used to calculate hourly voltage variations across each segment of the distribution network, providing insights into the system's operational stability and efficiency under varying load conditions.

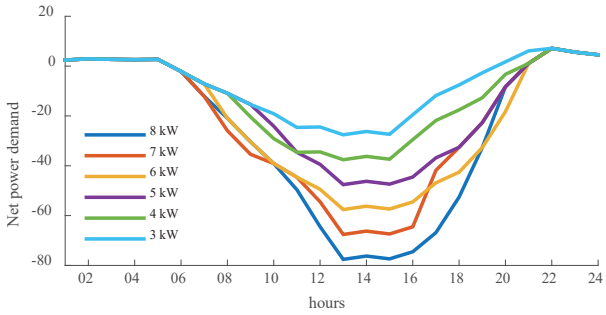

Fig. 3. Net power demand over a 24-hour for PV production from 3 kW to 8 kW.

D. Reference Values

For all nodes in the network, the following reference values are used:

- Nominal Voltage: Uref=400 V, representing the base operating voltage of the LV network,
- Power Factor: cosφ = 0.95, reflecting typical power factor values in residential networks.

These values are essential for ensuring that calculations align with the standard operational parameters of the network.

E. Voltage Analysis

An algorithm is implemented to calculate the voltage across all network segments. The algorithm iteratively evaluates whether the voltage at each node remains within +5% (-10%) of the reference voltage (U_{ref}). Voltage drops exceeding this range indicate that corrective measures, such as upgrading cables or redistributing loads, are necessary.

The voltage drop (ΔU) along a segment is calculated using the following formula:

$$\Delta U = I \cdot Z. \quad (2)$$

where:

I: The current through the segment,

Z: The impedance of the cable.

Impedance is determined based on the cable's length, cross-sectional area, and material properties.

The mathematical model is presented through the following expressions, which define the power flow calculations in the network based on fundamental electrical relationships.

The reactive power at node *i* is calculated based on the active power and power factor using the following equation:

Maja Muftić Dedović, Samir Avdaković, Adin Memić, PV Integration in LV Networks and Capacity Analysis, Journal of Energy, vol. 73 Number 4 (2024), 3–11
https://doi.org/10.37798/2024734698

$$Q(i) = P(i) \cdot \tan(\varphi) \quad (3)$$

where:

cos φ: Power factor at the given node.

P(i): The active power at the given node.

Q(i): The reactive power at the given node.

To determine the voltage drop, the total active and reactive power at node i must be define as the sum of all preceding nodes in the network:

$$P_{total}(i) = \sum_{j=1}^{n} P(j) \quad (4)$$

$$Q_{total}(i) = \sum_{j=1}^{n} Q(j) \quad (5)$$

The overall phase angle of the system is determined using the ratio of total reactive power to total active power:

$$\tan \varphi_{total}(i) = \frac{Q_{total}(i)}{P_{total}(i)} \quad (6)$$

where:

P_{total}: Total active power at node i.

Q_{total}: Total reactive power at node i.

φ_{total}: Total phase angle at node i.

$P(j)$: Active power at node j.

$P(j)$:Reactive power at node j.

n: Total number of nodes in the network.

The calculation of cable impedance includes the series resistance R and reactance X, considering the total phase angle. Effective impedance of the cable directly influences the voltage drop in the network:

$$Z_{aux} = R + X \cdot \tan \varphi_{total}(i) \quad (7)$$

The voltage drop along the cable is determined using the following equation:

$$\Delta U = \frac{1000 \cdot P_{total}(i) \cdot L(i) \cdot Z_{aux}}{U(i-1)^2} \quad (8)$$

where:

P_{total}: Total active power at node i.

$L(i)$: Length of the cable between nodes i-1 and i.

$U(i\text{-}1)$: The voltage at the previous node.

The implemented algorithm is illustrated in the following figure, which provides an overview of the steps for calculating voltage drops using MATLAB software [30]. The algorithm iterates over 24 hours, taking into account active and reactive power at each node, total power calculations, and the resulting voltage drop at each segment.

Algorithm 1: Algorithm for Node Voltage Calculation in Distribution Networks

Input: Active power vector `P`, number of nodes `n`, `cos_phi` vector, cable resistances `R` and reactances `X` per unit length, cable lengths `L`, base voltage `U_base`.

Output: Voltage matrix `U_matrix` for all nodes over 24 hours.

```
for t = 1 to 24 do
    Extract active power vector P for hour t.
    Reactive Power and Tangent Phi Calculation:
    for i = 2 to n do
        if P(i) == 0 then
            Set tg_phi(i) = 0.
        else
            Compute reactive power Q(i) = P(i) * tan(acos(cos_phi(i))).
            Compute tg_phi(i) = Q(i) / P(i).
        end
    end
    Total Power Calculation:
    for i = 1 to n do
        for j = i to n do
            Accumulate P_total(i) += P(j).
            Accumulate Q_total(i) += Q(j).
        end
        if P_total(i) == 0 then
            Set tg_phi(i) = 0.
        else
            Compute tg_phi(i) = Q_total(i) / P_total(i).
        end
    end
    Voltage Drop and Node Voltage Calculation:
    for i = 2 to n do
        Compute auxiliary variable:
            Z_aux = R + X · tg_phi(i).
        if P_total(i) == 0 then
            Set ΔU = 0.
        else
            Compute voltage drop:
            ΔU = (1000 · P_total(i) · L(i) · Z_aux) / U(i-1)^2.
        end
        Update node voltage:
            U(i) = U(i-1) - ΔU · U(i-1).
    end
    Store U in U_matrix for hour t.
end
Output:
Return U_matrix.
```

F. Conductor Capacity Verification

The current flowing through each network segment is evaluated to ensure it does not exceed the continuous current-carrying capacity (I_{th}) of the cable. For this study, the threshold is set to I_{th}=192A.

The verification process involves:

Maja Muftić Dedović, Samir Avdaković, Adin Memić, PV Integration in LV Networks and Capacity Analysis, Journal of Energy, vol. 73 Number 4 (2024), 3–11
https://doi.org/10.37798/2024734698

1. Determining Cable Specifications: Cable specifications, including the permissible current-carrying capacity under steady-state conditions, are obtained from manufacturer data or relevant standards. Factors such as ambient temperature, installation method, and cable insulation are considered.
2. Calculating Current Flow: The current through each segment is calculated as:

$$I = P/(\sqrt{3} \cdot V \cdot \cos\varphi). \quad (9)$$

where:
P: Power flow through the segment,
U: Voltage level,
cosφ: Power factor.

3. Comparison with Capacity: The calculated current is compared to I_{th}. If $I>I_{th}$, the cable is insufficient, and recommendations for upgrading are provided.

This verification ensures the thermal safety of the conductors and prevents overloading, which could lead to insulation failure or fire hazards.

G. Iterative Optimization Process

An iterative process is applied to optimize the integration of PV. If both voltage and current limits are within acceptable ranges, the installed PV capacity is incrementally increased by 1 kW from 3 to 8 kW. This process continues until one or more constraints are violated, marking the maximum permissible PV capacity for the network. If constraints are exceeded at the initial stage, the analysis concludes with recommendations for network reinforcement or alternative strategies.

The iterative optimization process determines the maximum PV capacity that the network can accommodate while ensuring voltage and current constraints are not violated. The process follows an incremental approach where the PV capacity is increased in steps of ΔP=1 kW, starting from the initial production $P_{PV,initial}$. The updated PV production at each iteration is given by:

$$P_{PV,new} = P_{PV,prev} + \Delta P \quad (10)$$

At each step, the voltage and current limits are checked:

$$U_{max}(i) < U_{th}, \; I_{max}(i) < I_{th} \quad (11)$$

where U_{th} and I_{th} represent the permissible voltage and current limits, respectively. If these conditions are met, the iteration continues with an increased PV production. If one or both constraints are exceeded, the process terminates, identifying the maximum allowable PV production for the given network configuration.

IV. Day-Ahead PV Output Prediction and Capacity Analysis Using Neural Networks

In this section of the paper, a scientific approach is taken to predict day-ahead PV power output and voltage variations on LV networks, as well as to conduct capacity analysis based on PV production data available for the forecasted day. The integration of PV systems into power networks plays a critical role in transitioning towards sustainable energy systems [31]. Accurate predictions of PV output are essential for optimizing the operation and planning of energy systems, ensuring grid stability, and maximizing the utilization of renewable energy sources, as demonstrated in [32]

The predictive model for PV output utilizes a feedforward neural network (FNN), which is selected for its computational efficiency and ability to capture non-linear relationships between input variables. The model is trained using historical data of PV production and meteorological variables, including solar irradiance, temperature, and cloud cover. These variables are chosen because of their significant impact on PV system performance. The prediction system is developed for six PV systems with nominal capacities ranging from 3 kW to 8 kW.

The neural network architecture includes a single hidden layer with 10 neurons to balance complexity and computational cost. A non-linear activation function, such as sigmoid, is applied in the hidden layer to model complex interactions between inputs, while the output layer employs a linear activation function to produce continuous predictions of PV power output. The Levenberg-Marquardt backpropagation algorithm, a robust optimization method, is used for training. The training process is conducted in MATLAB [30] using the built-in train function.

The input dataset for the neural network consisted of 24 hourly values of PV production for each system, representing typical operational data for one day. Additionally, three key meteorological variables are included: solar irradiance, temperature, and cloud cover. Solar irradiance, measured in watts per square meter (W/m²), represents the amount of solar energy available to the PV, with values ranging from 0 (night) to 1000 W/m² (peak sunlight). Ambient temperature, measured in degrees Celsius (°C), affects panel efficiency and ranged from 5°C in the early morning to 32°C in the afternoon. Cloud cover, expressed as a percentage, is used to estimate the impact of cloudiness on solar availability, with values ranging from 0% (clear skies) to 100% (fully overcast).

To ensure efficient training and prevent biases caused by scale differences among the input variables, all meteorological inputs are normalized to a range of [0, 1].

The input data matrix X is constructed by combining the hour of the day (1 to 24), normalized solar irradiance, normalized temperature, and normalized cloud cover. The target output matrix Y consisted of historical PV production values for each system.

The neural network is trained using this dataset, with the loss function defined as the mean squared error (MSE) between predicted and actual outputs. The training process iterated for up to 100 epochs or until the model achieved convergence, defined as the minimization of MSE to a predefined threshold.

After training, the model generated day-ahead predictions for each PV system using the same meteorological conditions. These predictions are then utilized for additional analyses, including voltage drop simulations on low-voltage networks and capacity assessments of the PV systems under forecasted conditions.

V. Results and Discussion

The proposed methodology is tested on an LV distribution network model. The results demonstrated that:

1. Voltage remained within +5% (-10%) of the nominal voltage for most scenarios.
2. Current levels are below the continuous current-carrying capacity of the cables, ensuring thermal safety.

Maja Muftić Dedović, Samir Avdaković, Adin Memić, PV Integration in LV Networks and Capacity Analysis, Journal of Energy, vol. 73 Number 4 (2024), 3–11
https://doi.org/10.37798/2024734698

3. Incremental increases in PV capacity allowed for a gradual understanding of the network's limitations.

The results obtained by applying the approach explained in Section III are presented for two cases. The first case utilizes modeled PV production data.

The second case considers forecasted PV production one day ahead, as described in Section IV. Figure 4. illustrates the results for the first case, while Table 1. presents the outcomes for the second case, highlighting the relationship between PV production and voltage levels (U) across various scenarios.

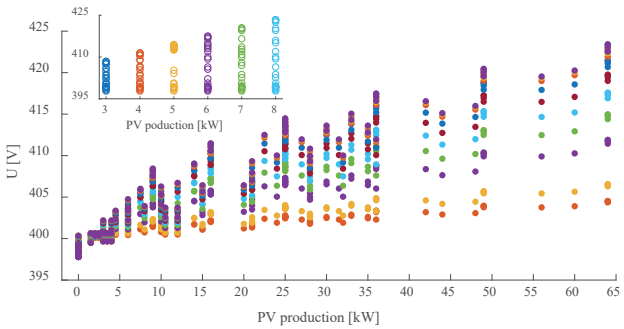

Fig. 4. Relationship between PV production and voltage levels (U) across various scenarios.

Table I

Comparison of Voltage (%) for Modeled and Forecasted PV Production at Different Power Levels

PV Production (kW)	Modelled Voltage (%)	Forecasted Voltage (%)	Difference (%)
3	2.11	2.03	0.08
4	2.87	2.92	0.05
5	3.62	3.74	0.12
6	4.37	3.97	0.4
7	5.11	5.25	0.14
8	5.85	5.79	0.06

From the approach provided in section III, it is evident that the voltage levels across the network are significantly influenced by the size of the PV systems, ranging from 3 kW to 8 kW. The voltage levels tend to increase slightly with higher installed PV capacities due to the reverse power flow in scenarios where local generation exceeds demand. For instance, at a PV size of 3 kW, the observed voltage levels are predominantly between 400 V and 405 V, while for larger systems like 8 kW, voltage levels range between 415 V and 420 V. This increase demonstrates that higher PV capacities inject more power into the network, improving voltage profiles but also necessitating careful voltage regulation to avoid overvoltage issues. Crucially, the voltage values for all PV capacities remain within the permissible range of +5% of -10 % of the nominal voltage (400 V), confirming that the LV network is capable of integrating these capacities without breaching operational voltage limits.

The voltage along the network is calculated for a cable length of 500 meters. This length contributes to increased impedance, amplifying voltage variations under higher loads, especially during peak consumption periods. Despite this, the results indicate that the network generally maintains adequate voltage under most conditions. For instance, at a 3 kW PV production level, voltage variations remain minimal, with average below 2 V, demonstrating a well-balanced network response. However, at higher capacities, such as 8 kW, maintaining acceptable voltage levels becomes more challenging. While the average voltage drop across nodes is approximately 8.5 V, there are instances where the maximum voltage drop exceeds the critical threshold of 20 V. This highlights a potential risk of exceeding acceptable voltage levels at higher levels of distributed generation, particularly under certain load and generation configurations.

The variation in voltage across the network depends on the installed PV production, with higher capacities leading to increased voltage fluctuations. Table II presents the voltage observed in the network for different PV production levels.

Table II

Voltage in the Network for Different PV production

PV Production (kW)	Voltage (V)
3	408.44
4	411.48
5	414.49
6	417.48
7	420.46
8	423.42

To address these challenges and ensure reliable network operation, especially in scenarios with higher PV penetration, optimization measures are essential. The integration of ESS, such as batteries, could help mitigate voltage fluctuations by absorbing excess generation during peak production and releasing energy during periods of high demand. Additionally, network interconnectivity and reinforcement, including meshing LV networks or upgrading conductor capacities, could reduce impedance and stabilize voltage profiles.

Furthermore, the implementation of advanced digital solutions, such as real-time monitoring and control systems, would enable timely detection of voltage deviations and facilitate rapid corrective actions. Digitalizing the management of distributed generation through smart inverters and automated demand response could dynamically adjust generation and consumption patterns to maintain voltage within acceptable limits.

These strategies emphasize the importance of a proactive approach to grid management, particularly as PV penetration continues to increase. A combination of optimization, ESS, network upgrades, and digitalization will ensure that acceptable voltage levels are maintained, even under demanding conditions. Such measures are critical for transitioning toward a resilient, sustainable, and future-ready power distribution system.

As PV sizes increase, voltage at the nodes gradually rises, particularly during periods of high solar irradiance, as power is injected into the network. This phenomenon is most evident for systems between 6 kW and 8 kW, where voltage levels at distant nodes are observed to peak around 420 V, compared to closer nodes which maintain voltages near 410 V. Hourly data trends further validate these findings, showing a stable voltage profile across multiple days. During peak production hours, typically midday, the voltage increases across the network are more uniform, whereas during early morning or evening hours, when PV generation is lower, the network operates closer to its base voltage of 400 V.

The results also indicate that the observed current values remain consistently below the maximum permissible limit of 192 A for XP00-A conductors. At peak conditions with an 8 kW PV system, the maximum current observed is approximately 120 A,

Maja Muftić Dedović, Samir Avdaković, Adin Memić, PV Integration in LV Networks and Capacity Analysis, Journal of Energy, vol. 73 Number 4 (2024), 3–11
https://doi.org/10.37798/2024734698

providing sufficient headroom for safe operation. Similarly, for lower capacities such as 3 kW, current levels are typically below 50 A, highlighting the efficiency of the network under partial loading conditions. Table III presents the maximum observed current for different PV production, ensuring that all values remain below the permissible thermal limit of 192 A.

TABLE III

MAXIMUM CURRENT IN CONDUCTORS FOR DIFFERENT PV PRODUCTION

PV Production (kW)	Max. Current (A)
3	41.83
4	57.43
5	72.34
6	87.47
7	102.39
8	117.44

Lastly, the analysis of integration capacity demonstrates that incremental increases in PV capacities, from 3 kW to 8 kW, allow the network to integrate distributed generation effectively while maintaining reliability. However, further increases in PV capacity beyond 8 kW may necessitate network reinforcements, such as upgrading conductor cross-sectional areas or transformer capacities, to ensure continued compliance with voltage and current limits.

These results from Table 1. demonstrate that the forecasted voltage closely align with the modeled values, with variations remaining within acceptable ranges. However, at higher PV production levels, the voltage drops approach critical thresholds (20 V and above), indicating a potential risk of exceeding acceptable voltage limits.

For a PV production of 3 kW, the modeled voltage drop corresponds to 8.44 V, while the forecasted drop is 8.12 V, with a negligible difference of 0.32 V. At 4 kW, the modeled drop increases to 11.48 V, and the forecasted value closely aligns at 11.68 V, resulting in a minor difference of 0.20 V. Similarly, at 5 kW, the modeled drop is 14.48 V, compared to the forecasted value of 14.96 V, with a difference of 0.48 V.

As the power level increases to 6 kW, the modeled voltage drop is 17.48 V, while the forecasted value is slightly lower at 15.88 V, resulting in a larger difference of 1.60 V. For 7 kW, the modeled and forecasted drops are 20.44 V and 21.00 V, respectively, with a difference of 0.56 V. Finally, at 8 kW, the modeled voltage drop is 23.40 V, and the forecasted value is nearly identical at 23.16 V, showing an excellent match with a minor difference of 0.24 V.

This underscores the importance of implementing measures such as energy storage, enhanced grid interconnectivity, and real-time monitoring to mitigate the impact of high PV penetration on maintaining acceptable voltage levels in the network.

The transformer under consideration has a nominal capacity of 160 kVA, equivalent to approximately 152 kW at a power factor of 0.95, typically feeding a LV network with four outgoing feeders. This analysis focuses on one feeder with 10 connections, where individual loads range from 3 kW to 8 kW, corresponding to feeder loads between 30 kW and 80 kW. This load represents approximately 19.7% to 52.6% of the transformer's total capacity, which is within operational limits, provided the total load across all feeders does not exceed 152 kW. Assuming equal distribution, the nominal load per feeder would be 38 kW, however, one feeder with a load of up to 80 kW would require reduced loads on the remaining feeders to prevent overloading. Voltage regulation, with a short-circuit voltage of 4%, remains adequate, but high feeder loads, especially with long cable lengths, could result in critical voltage variations. At a power factor of 0.95, the current for an 80 kW load reaches approximately 121 A, requiring careful impedance considerations to maintain voltage compliance within the allowable +5% (-10%) range of 400 V. While copper losses of 2.35 kW and iron losses of 0.46 kW indicate efficient operation under nominal conditions, sustained operation near maximum capacity could increase thermal stress, necessitating adequate cooling and monitoring to prevent insulation degradation. Proper load management and redistribution, along with voltage analysis and future scalability considerations, are essential, particularly if additional PV generation or higher loads are integrated. Incorporating reactive power compensation, monitoring, and automation can enhance operational reliability and prevent system overload.

The proposed methodology provides insights for grid operators in determining the maximum permissible PV hosting capacity in LV networks. However, its implementation in real-world scenarios requires considerations related to cost and complexity. The computational approach used in this paper, based on voltage and conductor capacity verification, can be integrated into existing distribution network planning tools to support decision-making processes. While the methodology itself is straightforward, its practical application may involve additional investments in monitoring infrastructure and advanced control systems to manage higher PV penetration levels effectively. Regulatory support and incentive structures may be required to encourage grid operators to adopt such analytical approaches in routine operations.

In real-world applications, PV generation is influenced by factors such as cloud cover, shading, panel aging, and seasonal variations, leading to deviations from expected production levels. These fluctuations can impact voltage profiles and the overall capacity of PV systems to offset household consumption. Lower-than-expected PV output may reduce the extent of voltage rise but can also limit the benefits of distributed generation in reducing grid dependence.

To account for these uncertainties, future research should explore probabilistic modeling approaches that incorporate variability in solar irradiance and load fluctuations. Integrating real-time monitoring and adaptive control mechanisms could help mitigate the effects of variable PV output, enhancing overall system stability and efficiency.

VI. CONCLUSION

This research analyzed the integration of PV systems into LV networks, focusing on voltage and conductor capacity. Using a systematic approach, the study demonstrated that PV capacities up to 8 kW could be integrated effectively while maintaining voltage levels within the permissible range (+5%, -10% of 400 V) and ensuring that conductor currents remain below thermal limits.

Key findings indicate that:

1. The tested conditions maintain acceptable voltage variations in the LV network, even at higher levels of PV penetration. However, the approach highlights the risk of overvoltage issues in scenarios of peak solar irradiance, particularly for systems exceeding 8 kW capacity.
2. Forecasted PV production values, obtained through neural network-based predictions, closely align with modeled data, showcasing the reliability and accuracy of the predictive model.

To address potential challenges in scenarios with increased PV

Maja Muftić Dedović, Samir Avdaković, Adin Memić, PV Integration in LV Networks and Capacity Analysis, Journal of Energy, vol. 73 Number 4 (2024), 3–11
https://doi.org/10.37798/2024734698

penetration, the following recommendations are proposed:

- Incorporation of ESS to absorb excess energy during peak production and release it during periods of high demand, mitigating voltage fluctuations.
- Network upgrades such as increasing conductor cross-sectional areas or upgrading transformers, are critical to support higher PV capacities.
- Implementing real-time monitoring and control systems, including smart inverters and automated demand response, will enhance the dynamic management of voltage and current levels.
- Policymakers and grid operators should adopt iterative and predictive methodologies for network design, ensuring long-term scalability and reliability.

By adopting these strategies, LV networks can support the transition to renewable energy systems while maintaining operational efficiency and stability. Future research should explore dynamic hosting capacity models and integrate stochastic methods to better account for uncertainties in load and generation patterns. This will further enhance the adaptability and resilience of power distribution systems in the face of growing renewable energy integration.

References

[1] Mahmud, K., M. J. Hossain, and G. E. Town, "Peak-load reduction by coordinated response of photovoltaics, battery storage, and electric vehicles," IEEE Access, vol. 6, pp. 29353–29365, 2018, doi: 10.1109/ACCESS.2018.2837144

[2] Siddiqui, A. S., and S. A. Siddiqui, "Ambiguities and nonmonotonicities under prosumer power: Optimal distributed energy resource investment in a deregulated electricity industry," Top, vol. 30, no. 3, pp. 492–532, 2022, https://doi.org/10.1007/s11750-022-00628-2

[3] Arnone, D., M. Cacioppo, M. G. Ippolito, M. Mammina, L. Mineo, R. Musca, and G. Zizzo, "A methodology for exploiting smart prosumers' flexibility in a bottom-up aggregation process," Appl. Sci., vol. 12, no. 1, Art. no. 430, 2022, https://doi.org/10.3390/app12010430

[4] May, R., and P. Huang, "A multi-agent reinforcement learning approach for investigating and optimising peer-to-peer prosumer energy markets," Appl. Energy, vol. 334, Art. no. 120705, 2023, https://doi.org/10.1016/j.apenergy.2023.120705

[5] Mahmud, K., B. Khan, J. Ravishankar, A. Ahmadi, and P. Siano, "An internet of energy framework with distributed energy resources, prosumers and small-scale virtual power plants: An overview," Renew. Sustain. Energy Rev., vol. 127, Art. no. 109840, 2020, https://doi.org/10.1016/j.rser.2020.109840

[6] Karalus, S., B. Köpfer, P. Guthke, S. Killinger, and E. Lorenz, "Analysing grid-level effects of photovoltaic self-consumption using a stochastic bottom-up model of prosumer systems," Energies, vol. 16, no. 7, Art. no. 3059, 2023, https://doi.org/10.3390/en16073059

[7] Umer, K., Q. Huang, M. Khorasany, W. Amin, and M. Afzal, "A novel prosumer-centric approach for social welfare maximization considering network voltage constraints in peer-to-peer energy markets," Int. J. Electr. Power Energy Syst., vol. 147, Art. no. 108820, 2023, https://doi.org/10.1016/j.ijepes.2022.108820

[8] Hashmi, M. U., D. Deka, A. Bušić, and D. Van Hertem, "Can locational disparity of prosumer energy optimization due to inverter rules be limited?," IEEE Trans. Power Syst., vol. 38, no. 6, pp. 5726–5739, 2022, doi:10.1109/TPWRS.2022.3223842

[9] Choi, S., K. Park, and S.-O. Shim, "Comparing validity of risk measures on newsvendor models in open innovation perspective," J. Open Innov. Technol. Market Complex., vol. 4, no. 1, pp. 1–12, 2018, https://doi.org/10.1186/s40852-017-0078-8

[10] Avau, M., N. Govaerts, and E. Delarue, "Impact of distribution tariffs on prosumer demand response," Energy Policy, vol. 151, Art. no. 112116, 2021, https://doi.org/10.1016/j.enpol.2020.112116

[11] Yang, J., M. R. Alam, W. Tushar, and T. K. Saha, "Incentivizing prosumer voltage regulation for unbalanced radial distribution networks," IEEE Trans. Sustain. Energy, vol. 15, no. 1, pp. 81–94, 2023, doi: 10.1109/TSTE.2023.3274154

[12] Wasiak, I., M. Szypowski, P. Kelm, R. Mieński, A. Wędzik, R. Pawełek, M. Małaczek, and P. Urbanek, "Innovative energy management system for low-voltage networks with distributed generation based on prosumers' active participation," Appl. Energy, vol. 312, Art. no. 118705, 2022, https://doi.org/10.1016/j.apenergy.2022.118705

[13] Nazaripouya, H., "Integration and control of distributed renewable energy resources," Clean Technol., vol. 4, no. 1, pp. 149–152, 2022, https://doi.org/10.3390/cleantechnol4010010

[14] Ali, A., K. Mahmoud, and M. Lehtonen, "Maximizing hosting capacity of uncertain photovoltaics by coordinated management of OLTC, VAr sources and stochastic EVs," Int. J. Electr. Power Energy Syst., vol. 127, Art. no. 106627, 2021, https://doi.org/10.1016/j.ijepes.2020.106627

[15] Zafar, R., A. Mahmood, S. Razzaq, W. Ali, U. Naeem, and K. Shehzad, "Prosumer based energy management and sharing in smart grid," Renew. Sustain. Energy Rev., vol. 82, pp. 1675–1684, 2018, https://doi.org/10.1016/j.rser.2017.07.018

[16] Yang, J., W. Tushar, T. K. Saha, M. R. Alam, and Y. Li, "Prosumer-driven voltage regulation via coordinated real and reactive power control," IEEE Trans. Smart Grid, vol. 13, no. 2, pp. 1441–1452, 2021, doi: 10.1109/TSG.2021.3125339

[17] Clastres, C., O. Rebenaque, and P. Jochem, "Provision of demand response by French prosumers with photovoltaic-battery systems in multiple markets," Energy Syst., vol. 14, pp. 869–892, 2023, doi: 10.1007/s12667-021-00482-4.

[18] Palacios-Garcia, E. J., A. Moreno-Muñoz, I. Santiago, I. M. Moreno-Garcia, and M. I. Milanés-Montero, "PV hosting capacity analysis and enhancement using high resolution stochastic modeling," Energies, vol. 10, no. 10, Art. no. 1488, 2017, https://doi.org/10.3390/en10101488

[19] Faranda, R., and H. Hafezi, "Reassessment of voltage variation for load power and energy demand management," Int. J. Electr. Power Energy Syst., vol. 106, pp. 320–326, 2019, https://doi.org/10.1016/j.ijepes.2018.10.012

[20] Hu, J.-L., and M.-Y. Chuang, "The importance of energy prosumers for affordable and clean energy development: A review of the literature from the viewpoints of management and policy," Energies, vol. 16, no. 17, Art. no. 6270, 2023, https://doi.org/10.3390/en16176270.

[21] Mieński, Rozmysław, Przemysław Urbanek, and Irena Wasiak, "Using energy storage inverters of prosumer installations for voltage control in low-voltage distribution networks," Energies, vol. 14, no. 4, Art. no. 1121, 2021, doi: 10.3390/en14041121.

[22] Torres, Igor Cavalcante, Daniel M. Farias, Andre LL Aquino, and Chigueru Tiba, "Voltage regulation for residential prosumers using a set of scalable power storage," Energies, vol. 14, no. 11, Art. no. 3288, 2021, doi: 10.3390/en14113288.

[23] Koirala, Arpan, Tom Van Acker, Reinhilde D'hulst, and Dirk Van Hertem, "Hosting capacity of photovoltaic systems in low voltage distribution systems: A benchmark of deterministic and stochastic approaches," Renewable Sustainable Energy Rev., vol. 155, Art. no. 111899, 2022, https://doi.org/10.1016/j.rser.2021.111899

[24] Koirala, Arpan, Tom Van Acker, Md Umar Hashmi, Reinhilde D'hulst, and Dirk Van Hertem, "Chance-constrained optimization based PV hosting capacity calculation using general polynomial chaos," IEEE Trans. Power Syst., vol. 39, no. 1, pp. 2284–2295, 2023, doi: 10.1109/TPWRS.2023.3258550

[25] Zobaa, Ahmed F., Shady H. E. Abdel Aleem, Sherif M. Ismael, and Paulo F. Ribeiro, eds., Hosting Capacity for Smart Power Grids, Berlin, Germany: Springer, 2020.

[26] J. S. Stein, C. P. Cameron, B. Bourne, A. Kimber, J. Posbic, and T. Jester, "A standardized approach to PV system performance model validation," in 2010 35th IEEE Photovoltaic Specialists Conference, Honolulu, HI, USA, June 2010, pp. 001079–001084, doi: 10.1109/PVSC.2010.5614696

[27] SMA Solar Technology AG, "Sunny Design," [Online]. Available: https://www.sunnydesignweb.com/sdweb/#/Home, Accessed on: Dec. 15, 2024.

[28] Public Enterprise Electric Utility of Bosnia and Herzegovina. "Documents and Forms," [Online]. Available: https://www.epbih.ba/eng/page/documents-and-forms. Accessed on: Dec. 15, 2024.

[29] Worlddata.info. "Energy consumption in Bosnia and Herzegovina," [Online]. Available: https://www.worlddata.info/europe/bosnia-and-herzegovina/energy-consumption.php. Accessed on: Dec. 25, 2024.

[30] MathWorks, Inc. "MATLAB R2024a," Natick, MA, USA, 2024. [Online]. Available: https://www.mathworks.com/products/matlab.html. Accessed on: Dec. 10, 2024.

[31] M. M. Dedović, S. Avdaković, A. Mujezinović, and N. Dautbašić, "Integration of PV into the Sarajevo Canton energy system—Air quality and heating challenges," Energies, vol. 14, p. 123, 2021. [Online]. Available: https://doi.org/10.3390/en14010123

[32] A. Memić, M. Muftić Dedović, N. Dautbašić, and M. Kapo, "Application of neural networks for predicting energy production from hybrid power systems considering the influence of stochastic weather changes," B&H Electr. Eng., vol. 18, no. 2, pp. 11–17, 2024, doi: 10.2478/bhee-2024-0006.

Journal of Energy

VOLUME 73 Number 4 | 2024

journal homepage: http://journalofenergy.com/

Diesel Engine Performance and Emission Properties using Kariya Biodiesel

Oluwafemi Emmanuel Ogundahunsi

Summary — **This study evaluated diesel engine performance and emission properties when fuelled with an already-produced kariya oil biodiesel (KOB) and KOB blends. This intends to explore KOB blends as a supplement in diesel engines. A hand-held exhaust gas analyzer was used to determine the gas emitted. In contrast, the brake power and exhaust gas temperature were determined using a Schenck W230 Eddy Current dynamometer and a thermometer respectively during the operation of the diesel engine fuelled with KOB. In contrast with standard petroleum-based diesel, the findings show that using KOB in diesel engines reduces CO and HC but increases NOx emitted due to its oxygenating property that aids fuel combustion. Also, with an increase in biodiesel blends, the fuel consumption increased, while the brake power and exhaust gas temperature decreased due to lower calorific value, higher viscosity, higher volumetric fuel per engine stroke, and the oxygen content dominating over lower calorific value for better combustion. From the study, both KOB B10 and B30 blends were considered optimally appropriate fuel supplements in a diesel engine. This study presents a proper way to manage the waste from kariya tree using it as a feedstock for biofuel production and diversifying different seeds through which biofuel can be produced.**

Keywords — **Biofuel, trans-esterification, bio-catalyst, exhaust gases, engines, emission properties**

I. Introduction

Biodiesel is produced via transesterification of vegetable oil or animal fat mixed with alcohol and a catalyst. Studies show that vegetable oil is a potential fuel in diesel engines due to its simple production process, ecologically friendliness, and similar physiochemical properties to petroleum-based diesel. However, it affects the durability of a diesel engine negatively when used directly. This is due to its high viscosity which thickens its oil lubricant and increases fuel droplets in the engine cylinder thereby leading to partial fuel combustion, excessive carbon build-up, and blockage of the combustion chamber [1]-[3]. To provide solutions to these challenges, some diesel engines were improved to heat the oil before its injection to enhance its atomization in the combustion chamber. Also, different research on the use of oil mixed with petroleum-based diesel as a supplementary fuel in diesel engines has been carried out. However, this blend only reduces the challenges but never eradicate them which make transesterification of vegetable oil needed before blending it with petroleum-diesel. Biodiesel produced through this process is then mixed with petroleum-based diesel to enhance its use in a diesel engine and to conform to the ASTM quality standard.

It is important to note that the use of edible oil seeds in biodiesel production constitutes a direct competition with their usage as food resulting in a reduction in food supply. Due to these limitations, unconventional oil seeds and wastes are being explored as feedstock in biodiesel production. Africa has great potential for biodiesel production based on its widespread diverse oil seed plants which are major feedstock for its production. Some of these oil-seeds already studied include: Luffa aegyptiaca Mill [4], [5], Ricinus communis [6], [7], Azadirachta indica [8], Jatropha curcas [9], [10] and Hevea brasiliensis [11]. And some unconventional oil-seeds which are non-edible but are good feedstock potential in producing biofuels include Delonix regia, Cypripedium acaule, Asclepias syriaca, Millettia pinnata, Sapindus mukorossi, and Helianthus annuus [12]-[14].

[15] studied the performance characteristics like; brake thermal efficiency, torque, fuel used, and power output of an internal combustion engine when fuelled with some biodiesel. It was discovered that biodiesels contain about 10 percent weight of oxygen. This oxygen enhances fuel combustion, yet it increases the amount of fuel consumed when the engine is in operation. The blends of Jatropha oil biodiesel with petroleum-based diesel gave a better brake thermal efficiency which rises from 27.4% to 28.7% [15].

Contrarily, [16] investigated sunflower, safflower, and rapeseed oil biodiesel fuel in diesel engines, and the power output was discovered to be similar to the power output of petroleum-based diesel but durability challenges were predicted as a result of the carbonizing effect. [17] investigate the effect of varied engine speeds at full and partial loads of a diesel engine comparing sunflower oil biodiesel with petroleum-based diesel as fuel during the operation. It was observed that sunflower biodiesel had a lower brake power and higher fuel consumption when compared with petroleum-based diesel. Nevertheless, biodiesel is preferred to petroleum-based diesel based on its lubricant properties which help the lifespan of the engine. Being an oxygenated fuel, biodiesel produces lower greenhouse gas emissions in a diesel engine than petroleum-based diesel.

Moreover, biodiesel is referred to as clean fuel because there is no production of SO_x and CO_2 in its emission during use. [18] evaluated the performance of tobacco seed oil biodiesel in a diesel engine and observed a rise in torque and power (having a lesser heating value of 39.8MJ/kg). Several experiments were carried out for indirect injection of biodiesel blends in diesel engines with

(Corresponding author: Oluwafemi Ogundahunsi)

Oluwafemi Ogundahunsi is with the Faculty of Engineering and Technology, First Technical University, Ibadan, Nigeria (e-mail: ogundahunsioluwafemi@gmail.com)

Oluwafemi Emmanuel Ogundahunsi, Diesel Engine Performance and Emission Properties using Kariya Biodiesel, Journal of Energy, vol. 73 Number 4 (2024), 12–15
https://doi.org/10.37798/2024734699

1500 and 3000rpm engine speeds. Despite the lower heating value that was observed with the use of biodiesel, the highest torque and power were observed when a 17.5 percent blend was used. An investigation was carried out by [19] to examine differently oxidized soybean oil biodiesel. The fuel consumption of pure, oxidized, and non-oxidized biodiesel increased to 15.1, 12, and 13.8 % respectively. The variation in the fuel consumed is attributed to the varied heating values of the biodiesels. [20] investigated linseed oil biodiesel performance in a diesel engine. In the research, an increase in thermal efficiency was observed particularly at lower loads.

In contrast, [21] observed a reduction in diesel engine efficiency when fueled with palm oil biodiesel of 0% and 20% blends, however, the slight variation (less than 2.3 percent in both cases) could be significant. It was also discovered that there was an increase in energy consumption. It was discovered that there was a power reduction at full load of the diesel engine at low speed and high speed of 5% to 10% reduction respectively [22].

Kariya seed oil has been found to be non-edible making it suitable for biodiesel production as it does not compete with human consumption [23]. The biodiesel produced from kariya seed oil has been found to be a good potential fuel to supplement petroleum-diesel in an internal combustion engine due to its fuel characteristics [24], yet the performance evaluation with emission properties of the engine while fuelled with this biodiesel is yet to be investigated in any literature. This study presents a proper way to manage the waste from kariya trees using it as a feedstock for biofuel production and diversifying different seeds through which biofuel can be produced.

II. Materials and Methods

The performance evaluation (fuel consumption, brake power, and exhaust gas temperature) of a diesel engine (Nulux R175A Diesel Engine) fuelled with KOB and its blends were determined. The performance of the diesel engine was examined using petroleum-based diesel (B0), prepared kariya biodiesel blends; B10 (10% biodiesel, 90% petrol diesel), B30 (30% biodiesel, 70% petrol diesel), B50 (50% biodiesel, 50% petrol diesel), B70 (70% biodiesel, 30% petrol diesel), and B90 (90% biodiesel, 10% petrol diesel), and biodiesel (B100) [24]. The brake power and the exhaust gas temperature were determined during operation using a Schenck W230 Eddy Current dynamometer and a thermometer respectively. Using a hand-held exhaust gas analyzer (Product Model: Aeroqual Series 500), emission characteristics also were determined; the rate of carbon monoxide, NOx, and hydrocarbon emissions. The results obtained when KOB blends were used were compared with that of pure petroleum-based diesel (B0).

III. Result and Discussion

The result obtained from the diesel engine performance when fueled with biodiesel blends revealed the behavior of each blend when used as fuel and it showed the appropriate blends for a diesel engine.

A. Emission characteristics

The emission characteristics result obtained when fueled with the produced KOB blend is shown in Fig. 1(a-c).

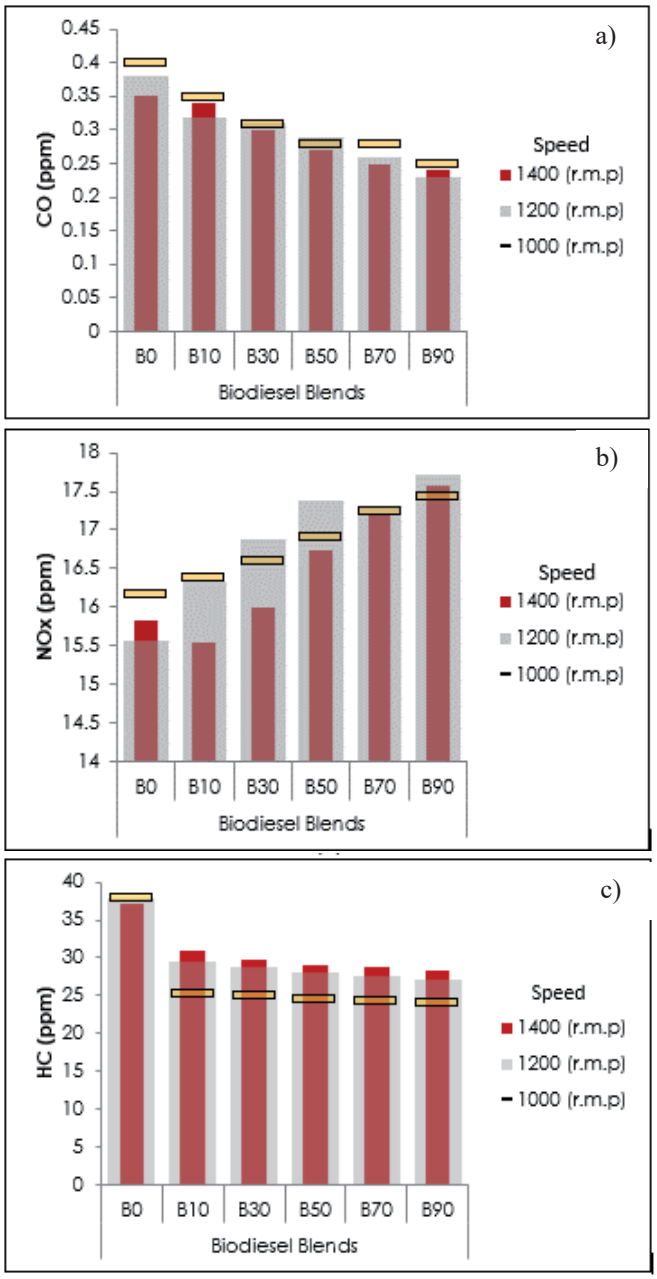

Fig. 1. Exhaust gas analysis vs. the biodiesel blends a) CO b) NOx c) HC

Figure 1a reveals that the carbon monoxide (CO) decreases as the biodiesel blends increase. A little increase in CO emitted was noticed with an increase in the engine speed. As the diesel engine operates at 1000 rpm, the CO emitted was reduced from 0.35 – 0.25, at 1200 rpm, the CO emitted was reduced from 0.32 – 0.23, and at 1400 rpm, the CO emitted was reduced from 0.34 – 0.24. It was observed that when petroleum-based diesel was used the CO emitted was higher than when biodiesel blends were used. The high cetane content and presence of oxygen in the biodiesel's molecular structure can be the cause for the drop in CO emissions that occur as the blend increases. This result implies that since the biodiesel produced contains some oxygen, it aids in fuel combustion, leading to a reduction in CO emitted.

The emission characteristics as shown in Fig. 1b show that the increase of biodiesel blends slightly increases the emission of NOx from 16.38 – 17.44 ppm for 1000 rpm, 16.34 – 17.71 ppm for 1200 rpm, and 15.55 – 17.58 ppm for 1400 rpm. However, there is a random variation of NOx emission through the biodiesel blends as the engine speed increases. The NOx emitted when fueled with petroleum-based diesel at all engine speeds is lower than NOx emitted

Oluwafemi Emmanuel Ogundahunsi, Diesel Engine Performance and Emission Properties using Kariya Biodiesel, Journal of Energy, vol. 73 Number 4 (2024), 12–15
https://doi.org/10.37798/2024734699

by all the biodiesel blends except at the speed of 1400 rpm when the B10 blend is lower than that of petroleum-based diesel. This result agrees with the findings of previous research on the effect of biodiesel on the NOx emissions which indicate a slight increase in NOx emitted when the biodiesel increases in the blend [19]. Some studies reveal no significant difference in NOx emitted when biodiesel increases in the blend. According to [8], the presence of monomers and polymers of unsaturated fatty acids in biodiesel can be the cause of an increase in NOx emitted. It can also be attributed to the presence of oxygen in the biodiesel which results in NOx formation that is majorly initiated by high cylinder temperature with its occurrence crank angle.

The result in Fig. 1c showed that hydrocarbon emitted by the engine decreases with the increase of biodiesel in the blend but increases with an increase in engine speed. It was discovered that the hydrocarbon emitted when petroleum-based diesel (B0) was used as fuel in the diesel engine was more compared to when biodiesel blends were used. The decrease in hydrocarbon emitted with an increase in biodiesel blends can also be attributed to the low viscosity and the oxygen content in the biodiesel produced leading to better combustion of the fuel. The increase in the hydrocarbon emitted when the engine speed increases may be associated with the increasing fuel quantity injected into the engine cylinder resulting in the fuel incomplete combustion thereby increasing hydrocarbon emitted. A similar trend was also observed with decreasing CO and HC and increasing NOx while operating the diesel engine with biodiesel produced using castor oil, soybean oil, rapeseed oil, sunflower oil, and olive oil ([1], [25], [14], [26]). Conversely, the NOx emitted decreased as the biodiesel increased in the blends when karanja oil, neem oil, jatropha, and sesame oil were tested in a diesel engine though a trend of decrease in CO and HC was observed [27].

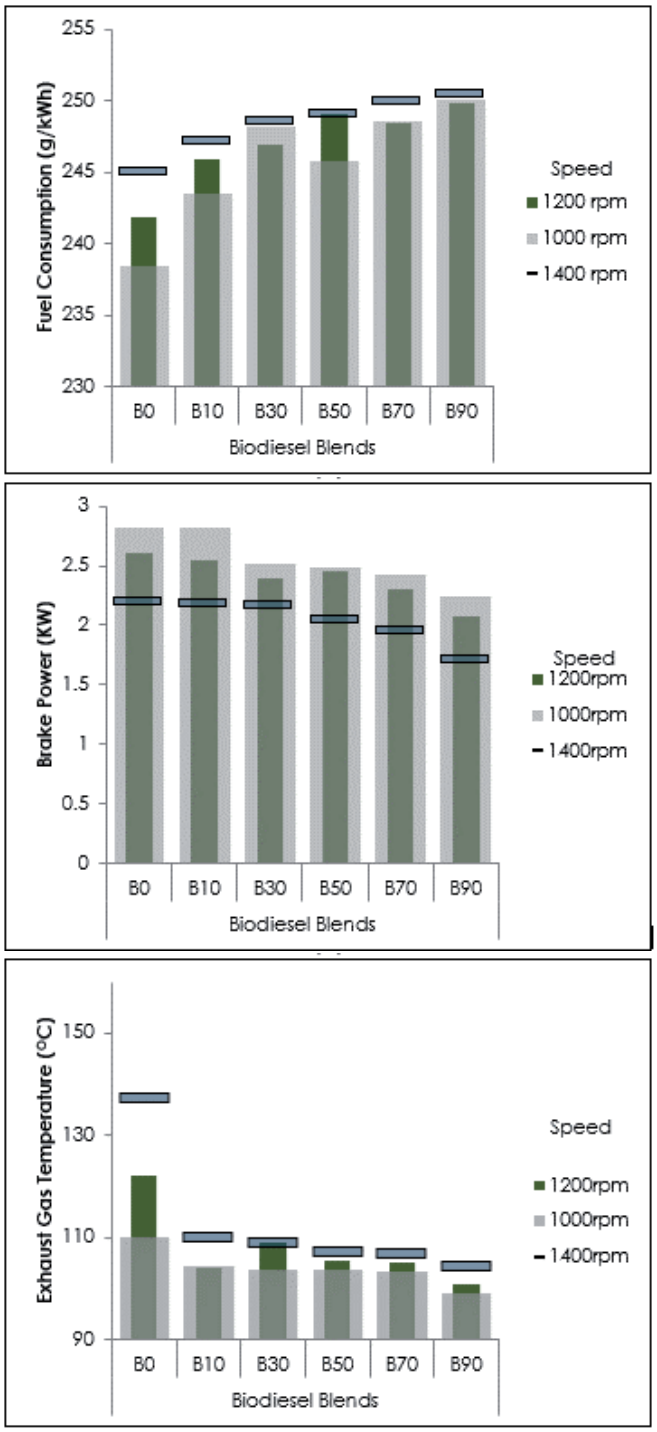

Fig. 2. Engine performance evaluation vs. the biodiesel blends: (a)Fuel Consumption (b) Brake Power
(c) Exhaust Gas Temperature

B. Performance evaluation

From Fig. 2a, it was observed that the fuel consumed by the engine increased as biodiesel increased in the blends between B10 and B90 from 243.53 – 250.08 g/kWh, 245.88 – 249.85 g/kWh, and 247.10 – 250.35 g/kWh for 1000, 1200, and 1400 rpm respectively. Also, it was observed that the fuel consumed by the engine increases as the engine speed increases except for a slight difference with B30 and B90. This increase may be attributed to the high quantity of fuel introduced into the engine cylinder. It was also discovered that the fuel consumed when KOB was used increased as the blend increased due to the lower calorific value, higher viscosity, and higher volumetric fuel delivery of KOB per engine stroke.

Figure 2b shows the relationship between the brake power and the biodiesel blend ratio concerning the engine speed. At an increasing profile of the blends in the biodiesel for 1000rpm, 1200rpm, and 1400rpm, the brake power of the engine decreases. From the result, there is no substantial difference between the brake power of petroleum-based diesel and B10 of the biodiesel blend. [28] explained that the decrease in the engine brake power as biodiesel increases in the blends can be because of the lower heating value of the biodiesel. A similar trend was observed for biodiesel obtained from corn oil, rapeseed oil, soybean oil, and sunflower oil [29].

The graphical relationship between the exhaust gas temperature and the biodiesel blends concerning engine speed is shown in Fig. 2c. From the result, it was discovered that at an engine speed of 1000 and 1400 rpm, the Exhaust gas temperature decreases from 104.25 – 99.07 °C, 109.98 – 104.23 °C respectively with an increase of biodiesel in the blends from B10 to B90 while at engine speed 1200 rpm, the exhaust gas initially drops at B10 and then rise at B30 and finally decrease as the biodiesel increase. The temperature of the exhaust gas emitted by petroleum-based diesel (B0) is higher compared to biodiesel blends and this indicates that in biodiesel, there is complete combustion that has taken place in the engine cylinder converting energy from the fuel to maximum useful work compared to petroleum-based diesel. There is an increase in the exhaust gas temperature when the speed increases because more fuel has been released into the cylinder and there is more combustion of the fuel which produces heat.

Oluwafemi Emmanuel Ogundahunsi, Diesel Engine Performance and Emission Properties using Kariya Biodiesel, Journal of Energy, vol. 73 Number 4 (2024), 12–15
https://doi.org/10.37798/2024734699

IV. Conclusion

When a diesel engine was fueled with kariya diesel blends, there was a reduction in the emission of CO and HC as biodiesel increased in the blends, however, there was a little more NOx emitted when biodiesel blends were used compared to when petroleum-based diesel was used. Also, the fuel consumed increases as biodiesel increases in the blends while the brake power and exhaust gas temperature are lesser when biodiesel is used compared to petroleum-based diesel. The oxygen content and low viscosity of the biodiesel produced aid complete fuel combustion thereby reducing the CO and HC emitted while increasing the NOx emitted. Also, the oxygen content with a lower calorific value of the biodiesel results in more fuel consumed compared to when petroleum-based diesel was used. The decrease in engine brake power as the biodiesel increases in the blend may be due to the lower heating value of biodiesel. It was noted that there was a decrease in exhaust gas temperature when the biodiesel increased in the blend because of the physicochemical properties of the fuel and the level of oxygen present in it. Based on these findings showing reduced NOx emitted and low fuel consumption, two of the blends of the kariya biodiesel produced i.e. B10 and B30 were more appropriate for use optimally in a diesel engine. For further study on this research, the result of the emission characteristics and the performance evaluation of the engine when fueled with KOB and its blends should be compared with the performance of the engine when fueled with another biodiesel.

References

[1] Sattanathan, R. (2013). Production of biodiesel from castor oil with its performance and emission test. *International Journal of Science and Research*, Vol. 4(1): 273-279.

[2] Sidibé, S.S., Blin, J., Vaitilingom, G., and Azoumah, Y. (2010). Use of crude filtered vegetable oil as a fuel in diesel engines state of the art: Literature Review. *Renewable and Sustainable Energy Review*, Vol. 14(9):2748-2759

[3] Jones, S.T., and Peterson, C.L. (2002). Using unmodified vegetable oils as a diesel fuel extender –A Literature Review by Graduate Research Assistant and Professor and Interim Head Department of Biological and Agricultural Engineering University of Idaho, Moscow, Idaho 83843.

[4] Bamgboye, A.I. and Oniya, O.O. (2012). Fuel properties of loofah (Luffa cylindrica L.) biofuel blended with diesel. *African Journal of Environmental Science and Technology*, Vol. 6(9): 346-352.

[5] Ajiwe, V.I.E., Ndukwe, G.I., and Anyadiegwu, I.E. (2005). Vegetable diesel fuels from Luffa cylindrica oil, its methyl ester, and ester-diesel blends. *Chemical Class Journal*, Vol. 2(1):1-4.

[6] Soliman, M.S., Mohamed, H. A., Abdelhafez, O. A., and Nassibe, A. M. (2014). Production and characterization of biodiesel fuels from castor oil utilizing methanol. *International Research Journal of Engineering Science, Technology and Innovation*, Vol. 3(2): 17-23.

[7] Deshpande, D.P., Urunkar, Y.D. and Thakare, P.D. (2012). Production of biodiesel from castor oil using acid and base catalysts. *Journal of Chemical Engineering and Technology*, Warananagar, Kolhapur, Ms, India, Vol. 2(8):51-56.

[8] Aransiola, E.F., Betiku, E., Ikhuomoregbe D.I.O. and Ojumu T.V. (2012). Production of biodiesel from crude neem oil feedstock and its emissions from internal combustion engines, *African Journal of Biotechnology*, Vol. 11(22):6178-6186.

[9] Folaranmi, J. (2013). Production of biodiesel (B100) from jatropha oil using sodium hydroxide as a catalyst. *Journal of Petroleum Engineering*, Vol. 13:1-6.

[10] Junfeng, Q., Haixlan, S. and Zhi, Y. (2010). Preparation of biodiesel from jatropha curcas oil produced by two-phase solvent extraction, *Journals of Bioresources Technology*, Vol. 101(18): 7036-42

[11] Ramadhas, A.S., Muraleedharan, C. and Jayaraj, S. (2005). Performance and emission evaluation of a diesel engine fueled with methyl esters of rubber seed oil. *Renewable Energy*. Vol. (30):1789–1800.

[12] Padmanabhan, S., Rajasekar, S., Ganesan, S., Saravanan, S. and Chandrasekaran, M. (2017). Performance and emission analysis on ci engine using Soapnut oil as biofuel. *ARPN Journal of Engineering and Applied Sciences*. Vol. 12, No. 8.

[13] Orhevba, B.A., Chukwu, O., Osunde, Z.D. and Ogwuagwu, V. (2013). Studies on the effect of pressure on yield of mechanically expressed neem seed kernel oil. *Global Journal of Engineering, Design, and Technology*, Vol. 2(5): 20-24.

[14] Labeckas, G. and Slavinskas, S. (2006). The effect of rapeseed oil methyl ester on direct injection diesel engine performance and exhaust emissions. *Energy Conversion and Management*, Vol. 47:1954–1967.

[15] Demirbas, A. (2009). Progress and recent trends in biodiesel fuels. *Energy Conversion and Management*; 50:14–34.

[16] Atiqah, B. N. (2012). Biodiesel from Various Vegetables and Tallow Oils. (An Unpublished B. Tech. Thesis, Department of Mechanical Engineering, Universiti Malaysia Pahang, Malaysia).

[17] Kapilan, N., Ashok Babu, T.P., Reddy, R.P. (2009). Technical aspects of biodiesel and its oxidation stability. *International Journal of Chemical Technology Research* CODEN (USA); 1(2):278–82 [ISSN: 0974-4290].

[18] Usta N. (2005). An experimental study on performance and exhaust emissions of a diesel engine fueled with tobacco seed oil methyl ester. *Energy Conversion and Management*; 46:2373–86.

[19] Lapuerta, M., Rodríguez-Fernández, J., Agudelo, J.R. (2008). Diesel Particulate Emissions from Used Cooking Oil Bio-diesel. *Bioresource Technology*. 99: 731-740.

[20] Agarwal, A.K., Das, L.M. (2001). Biodiesel development and characterization for use as a fuel in compression ignition engines. *Transaction of the ASME Journal of Engineering for Gas Turbine and Power*; 123:440–7.

[21] Lin, Y.C., Lee, W.J., Wu, T.S., Wang, C.T. (2006). Comparison of PAH and regulated harmful matter emissions from biodiesel blends and paraffinic fuel blends on engine accumulated mileage test. *Biofuel Journal*; 85:16–23.

[22] Kaplan, C, Arslan, R, Surmen, A. (2006). Performance characteristics of sunflower methyl esters as biodiesel. *Energy Source Part A*; 28:751–755.

[23] Ogundahunsi, O. E., B. S. Ogunsina, and E. F. Aransiola. (2022a). "Kariya Pod-Husks: A Novel Biocatalyst in Biodiesel Production". *Journal of Energy Research and Reviews* 11 (4):48-54. https://doi.org/10.9734/jenrr/2022/v11i430286

[24] Ogundahunsi, O. E., B. S. Ogunsina, and E. F. Aransiola. (2022b). "Kariya Biodiesel Process Optimization Using Kariya Pod-husks Bio-catalyzed". *Journal of Energy Research and Reviews* 11(4): 33-47. https://doi.org/10.9734/jenrr/2022/v11i430285

[25] Chang, H.M., Liao, H.F., Lee, C.C., Shieh, C.J. (2005) Optimized synthesis of lipase-catalyzed bio-diesel by Novozym 435 *Journal of Chemical Technology and Biotechnology* 80: 307-312.

[26] Kalligeros, S., Zannikos, F., Stournas, S., Lois, E., Anastopoulos, G., Teas, C., and Sakellaropoulos, F. (2003). An Investigation of Using Biodiesel/Marine Diesel Blends on the Performance of a Stationary Diesel Engine. *Biomass Bioenerg*. 24: 141-149.

[27] Raheman, H., and Phadatare, A.G. (2004). Diesel Engine Emissions and Performance from Blends of Karanja Methyl Ester and Diesel. *Biomass Bioenerg*. 27: 393-397.

[28] Otu, F.I., Bello, E.I., Ogedengbe, T.I, Lajide, L. (2018). Performance Evaluation of Rubber Seed Oil Biodiesel. *Journal of Engineering and Engineering Technology*. Vol. 12 (2): 124-130

[29] Abdullah, A., John, F., and Rob, B. (2011). The Effects of Using Biodiesel as Fuel on Compression Ignition (CI) Engine and Its Production from Vegetable Oils. 2011 *International Conference on Environmental, Biomedical and Biotechnology*. Vol. 16(11): 41-46.

[30] Jones, S.T., Peterson, C.L. and Thompson, J.C. (2001). Used vegetable oil fuel blend comparisons using injector coking in a diesel engine. Biological and Agricultural Engineering Department, University of Idaho, Moscow, Idaho. Presented at 2001 *ASAE Annual International Meeting*, Sacramento, Califonia, July 30– August 1, 2001. Society of Agricultural Engineering, Paper No. 01-6051.

Journal of Energy

VOLUME 73 Number 4 | 2024

journal homepage: http://journalofenergy.com/

The Roles of Battery Energy Storage System in Different Energy Communities

Filip Dimač, Ivan Rajšl, Sara Raos and Goran Ribić

Summary — This article analyses the concept of energy communities. Energy communities are basically divided into physical and virtual communities, and they are also differentiated according to business models. The development of these business models requires virtual connectivity enabled by digital platforms, smart grids and the Internet of Things. The advantages and disadvantages of energy communities are described, and the legal side is analysed. The role of battery storage in the energy community is described and the aim of this paper is to analyse the role of battery storage in different types of energy communities. A mathematical model has been described to analyse the viability of the battery in three energy communities with different consumption curves and the results obtained by simulation have been presented.

Keywords — energy communities, battery energy storage system, rooftop, PV solar system

I. Introduction

The energy transition process refers to changes in the way energy is produced and used, with the aim of reducing its price and its negative impact on the environment. The main reason for initiating the energy transition is climate change and the reduction of greenhouse gases. As a result of the energy transition, consumers are becoming active consumers – "prosumers" who not only draw energy from the grid but also make it available for others to use as needed. The development of information and communication technologies is making a significant contribution to the development of innovative management solutions [1]

Energy communities are proving to be one of the most suitable solutions for the integrating prosumers and their distributed sources. The application of this market-based mechanism can lead to a better local balance of supply and demand for electrical energy, reduce voltage deviations from nominal values and improve the welfare of the entire community. As part of the "Clean energy for all Europeans" package (2019), EU directives introduced new provisions for the organisation of the energy market and framework conditions for new energy initiatives. The framework for collective self-consumption is often defined separately from the provisions for energy communities due to its simplicity and significantly lower administrative and organisational requirements. [2] Three concepts are defined: collective self-consumption, renewable energy community and citizen energy community.

Energy communities can be implemented in different ways depending on various factors, but the simplest categorization is into physical and virtual energy communities. The main difference between the different types of energy communities lies in the way of using the power network and how the energy produced and consumed is billed and paid for. In the case of physical communities, a distinction can be made between collective self-consumption, i.e. consumers of their own renewable energy (private grid, e.g. neighborhood or residential building) and collective self-consumption (private and public grid). A virtual community is often defined as a regional community by its wider geographical context. [5]

Legislation can restrict the connection of members and thus the technical organisation of energy communities. An important aspect of energy communities is therefore to examine the legally permissible connections between participants before considering the technical aspects. In addition to the differences in the connection between participants, energy communities also differ in their business models. Research has identified and described six main archetypes and business models of energy communities. [4]

Battery energy storage systems (BESS) could solve many problems in electricity generation and distribution in the future. Generation from renewable energy sources (RES) is often dependent on weather conditions. Distributing the output of solar power plants (SPP) every hour or 15 minutes [12] is a challenge for the electricity system, which leads to an increased need for flexibility in the entire power system. In reference [9], the term flexibility of the electricity system was defined and the authors proved with their mathematical model that BESS have positive effects on systems with RES. Without RES, they reduce the need for peak load power plants, and with renewables they reduce the curtailment of renewable energy, but with BESS the flexibility of the electricity system was better. System flexibility was better with or without renewables when BESS was introduced.

The flexibility of power supply systems can be increased in many ways, including the intelligent use of electrical devices and the implementation of BESS. BESS are highly customisable and it is possible to choose the most suitable BESS solution for a specific purpose. Although BESS could be used to solve many problems related to energy systems, they are not yet widely used due to high costs and low profitability. Over the past decade, lithium-ion battery prices have fallen significantly and this trend is expected to continue. The decreasing cost of the battery makes it a more interesting solution and increases profitability.

In reference [3], the interaction of individual prosumers with the electricity grid was analysed and it was investigated how the

(Corresponding author: Goran Ribić)

Filip Dimač, Ivan Rajšl, and Sara Raos are with the Faculty of Electrical Engineering and Computing, University of Zagreb, Zagreb, Croatia (e-mails: filip.dimac@fer.hr, ivan.rajsl@fer.hr, sara.raos@fer.hr)

Goran Ribić is Tesla Ltd, Ivanec, Croatia (email: goran.ribic@tesla.com.hr)

Filip Dimač, Ivan Rajšl, Sara Raos and Goran Ribić , The Roles of Battery Energy Storage System in Different Energy Communities, Journal of Energy, vol. 73 Number 4 (2024), 16–25
https://doi.org/10.37798/2024734705

organisation of prosumers in energy communities affects their interaction with the grid. Individual prosumers independently invest and manage their own photovoltaic (PV) and BESS sources and buy and sell energy directly from the grid, while in the prosumer community the capacity and operation of the PV and BESS are optimised at the level of the entire community. The electricity generated in the community can be freely used by all members to meet demand at any given time or to charge any battery. The community also has the possibility to trade (buy and sell) electricity with the grid.

The high integration of photovoltaic systems can cause the problem of overvoltage in the grid. This problem can be solved through the use of BESS, usually connected in parallel with the photovoltaic power plant, and a system that manages the battery at the local level (household or community), taking into account the technical conditions of the grid, i.e. the conditions for maintaining voltage quality. Economic strategies of system management, whose goal is to maximise profits, ignore these conditions, but by intelligently using the overall potential of BESS, participants have the opportunity to offer services to grid operators in this way as well. Research [6] has shown that if the battery degradation factor is ignored, the battery will actually cause voltage problems. Restricting the operation of the battery to reduce its degradation will result in lower voltage spikes. In other words, battery-friendly operation is also grid-friendly operation. The schematic of the energy community with PV generation and a BESS is shown in Figure 1.

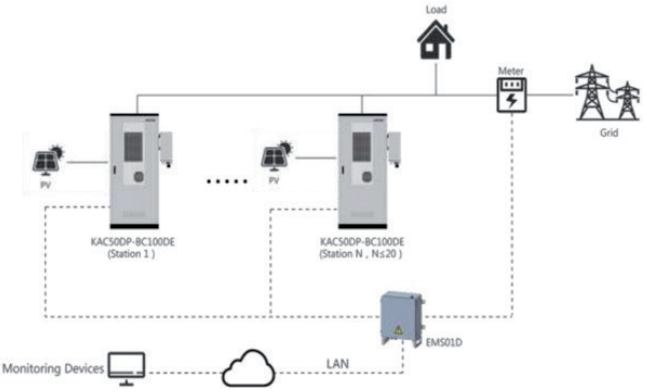

Fig. 1. BESS and PV integration scheme in the energy community [8]

The most common goal when installing BESS is to increase local self-consumption generated by photovoltaic systems. Although such systems reduce the amount of electricity exported to the grid from photovoltaic installations, there are many other benefits of the impact of batteries on the grid if they are properly managed. The BESS themselves have no influence on the production of photovoltaic power plants due to their temporal variability, but through their intelligent use it is possible to reduce peak consumption curves and thus relieve the grid and avoid grid congestion. This is possible by predicting generation from photovoltaic systems and consumption in households. Residential buildings are ideally suited to providing these services, as their consumption generally occurs at different times of day than the high output of the photovoltaic systems. This is in contrast to office buildings, where consumption is high during the day when generation from photovoltaic systems is also high. To maximise the economic benefit, the generation capacities and the battery must be correctly dimensioned based on the user's consumption. Generally, the production is dimensioned first and then the optimal battery capacity is determined.

This paper contributes to the evaluation of the role of battery systems in different energy communities. It also points out the advantages and disadvantages of the role of batteries in different energy communities. The rest of the paper is organised as follows: The evaluation approach and the applied software are presented in the Methodology chapter, while the Mathematical Model chapter presents the underlying mathematical expressions of the model. The results are presented and discussed in Chapter 4, Analysing battery storage in different types of energy communities, while Chapter 5 concludes the paper.

II. Methodology

The aim of this paper is to analyse the role of the BESS in different energy communities. For this purpose, three energy communities were designed and BESS was included in each of these three energy communities. The energy communities are differentiated by the seasonal electricity demand and the type of consumers that meet the needs of the communities themselves. Sometimes these communities may have a surplus of electricity. It is assumed that the surplus electricity generated can be sold at 80% of the current market price. The task is to perform a linear optimisation with a cost minimisation objective function that gives an optimal solution for each of the communities based on data on production, consumption, electricity prices, battery capacity, battery charging and discharging power and taking into account various constraints. Based on the optimisation solution, the municipalities can be compared and it can be shown in which type of municipality the use of BESS is most profitable. The Gurobi software package [13] was used to solve the optimisation problem. To perform the linear optimisation, data on annual electricity prices on the wholesale market on an hourly basis, data on annual consumption of electricity and thermal energy on an hourly basis and data on annual electricity generation from solar cells on an hourly basis are required. Data on electricity prices on the wholesale market in Croatia for the year 2023 on an hourly basis were used. [7]

To estimate electricity consumption, the nPRO software was used, which estimates heating, cooling and electricity requirements based on the geographical location, surface area and type of facility (kindergarten, school, hall, swimming pool, theatre, etc.). The facilities differ in terms of quantity and consumption curves. For more accurate modelling of heating, cooling and electricity demand for each type of facility, it is possible to manually enter data on specific annual consumption (kWh/m2/year) and total annual consumption (MWh). It is also possible to determine the start and end of the heating and cooling season, the percentage of heating for hot water production, the percentage of cooling for cooling the system and the percentage of heat recovery from heating losses. It is possible to make manual changes within the daily curve for each hour and each day of the week. Once all parameters have been set by pressing the "Calculate" button, the software outputs annual hourly consumption curves that can be created in an Excel document.

In order to cover the community's thermal energy requirements, it was assumed that the community uses heat pumps, as heat pumps use electricity to generate heat and therefore the entire energy requirement can be regarded as an electricity requirement, which greatly simplifies optimisation. The coefficient of performance (COP) indicates the ratio between the heat energy generated and the amount of electricity required by the heat pump for its work. In our case, we have assumed an efficiency of 3.

The SolarEdge [14] software was used to dimension the production capacity, which based on the geographical location, surface and slope of the roof, and on the basis of the type and slope of the photovoltaic panels, estimates how many photovoltaic panels can be installed on the roof, how many inverters are needed for the operation of the power plant and, ultimately, the production of the power plant. The software was used to

Filip Dimač, Ivan Rajšl, Sara Raos and Goran Ribić , The Roles of Battery Energy Storage System in Different Energy Communities, Journal of Energy, vol. 73 Number 4 (2024), 16–25
https://doi.org/10.37798/2024734705

estimate the roof and building areas, which is a necessary parameter for the nPro software that uses this data to estimate the consumption curves. The software was also used to estimate the number of photovoltaic panels that can be installed on the roofs, to estimate the maximum output of the photovoltaic power plant and to design a rooftop PV system. When dimensioning the production, the condition was taken into account that the production must not be higher than the peak consumption. When sizing all three communities, this was not the case at any time. Unfortunately, SolarEdge does not have the ability to generate Excel documents. For this reason, it was not used to obtain the annual hourly production curve required for further analysis.

Renewables.Ninja [15] [16] is a software that, based on the geographical location, the maximum DC or AC power of the photovoltaic power plant and the tilt of the panels, generates the annual hourly curves of the production of the photovoltaic power plant in the form of an Excel document.

The models of photovoltaic panels, inverters and battery storage in all communities are the same, but their sizing differs depending on the consumption of the communities themselves. The Trina Solar Vertex S TSM-DE09R.08 model was selected for the photovoltaic panel, 425 Wp efficiency 21.3%, dimensions 1762mm x 1134mm x 30mm and weight 21.8 kg. This photovoltaic panel was chosen for the reason that it has suitable dimensions and weight and is therefore easier to install, and the ratio of load on the roof and safety against strong winds and bad weather is optimal. In the first year, the panel loses 2% of its power, and then each time the power decreases by a maximum of 0.55%. The degradation factor must be taken into account when calculating the investment return.

The capacity of the battery storage is dimensioned based on the average electricity consumption during the night hours when there is no production in the community. The capacity to satisfy the eight-hour autonomy from 12 pm to 8 am was estimated.

The KSTAR 100kWh model was chosen for the battery storage. Battery storage always comes with its own converter.

Urban heat islands (UHI) represent increase of temperature inside of cities in regard to their rural environment, and with electricity production, photovoltaic panels have additional positive impact on thermal characteristics of the building on which they are installed by significantly lowering energy necessary for cooling inside the building. Panels block direct sun radiation which directly decreases roof temperature and wind drift between panels and roof additionally increases the positive effect by convection cooling. [10] Commonly, this important benefit is not taken into account when creating a mathematical model of a solar power plant, so we will not do it either, but it is important to point out that this positive effect will provide additional financial savings for all members of the energy community.

III. Mathematical Model

The goal of the model is to minimize the costs of the community that produces, consumes, stores, buys and sells energy in a period of one year.

The objective function of the optimization problem can be written as:

$$min \sum_{t=0}^{8760} price[t] * (B[t] - 0.8 * S[t]) \quad (1)$$

Where B is purchased energy, S is sold energy, *price*[*t*] is the price of electricity, and in the range of 0-8760 represents the number of hours in a year. The part of function price[t]∗(B[t]-0.8∗S[t]) represents expenses reduced for income.

The equation of balance between electricity consumption and production:

$$HH1ee[t] + HPe[t] = = \mathrm{B}[t] - S[t] + PV[t] + ch[t] - dch[t] \quad (2)$$

Variables:

B - purchased energy

S - sold energy

HP - thermal energy of the heat pump

HPe - heat pump electricity

ch - charging energy

dch - energy discharge

soe - battery charge status

x - charge discharge binary

XB - purchased energy binary

XS - sold energy binary

PV - production from photovoltaics

HH1ee - electricity consumption

HH1hd – heat demand

Constants:

$eff_{ch_{dch}} = 0.95$ =*charge/discharge efficien*
$COP = 3$ =*efficiency coefficient*
$Pmax$ =*battery discharge power*
$C =$ *battery capacity*
$HPmax$ = *maximum power of heat pumps*

In addition to consumption, production and price data, model constraints are also needed.

The constraints are:

1. State of charge of the batteries at the beginning and for all other hours:

$$soe[0] = 0 \quad (3)$$

$$soe[t] = soe[t-1] + ch[t] * eff_{ch_{dis}} - dch[t] * \left(\frac{1}{eff_{ch_{dis}}}\right) \quad (4)$$

2. The demand for thermal energy is met through heat pumps:

$$HPe[t] = HH1hd[t] * (1/COP) \quad (5)$$

3. Limitation of the maximum charging and discharging power and impossibility of charging and discharging at the same time:

$$ch[t] <= Pmax * X[t] \quad (6)$$
$$dh[t] <= Pmax * (1 - X[t]) \quad (7)$$

4.Limitationthatenergycannotbeboughtandsoldatthesametime:

$$B[t] <= M * XB[t] \quad (8)$$
$$S[t] <= M * XS[t] \quad (9)$$
$$XB[t] + XS[t] <= 1 \quad (10)$$

Filip Dimač, Ivan Rajšl, Sara Raos and Goran Ribić , The Roles of Battery Energy Storage System in Different Energy Communities, Journal of Energy, vol. 73 Number 4 (2024), 16–25
https://doi.org/10.37798/2024734705

Big number M (100,000) is used according to optimization practice in order to ensure that energy cannot be bought (charged) and sold (discharged) at the same time.

IV. Analysis of Battery Storage in Different Types of Energy Communities

A. Community 1

Community 1 consists of consumption, production and a BESS, and the community is located in the area of Zagreb. Consumers are: 40 apartments/apartments, a restaurant and a parking lot with a charging station for electric vehicles. The production is from photovoltaic panels that are placed on the roofs of all the mentioned buildings. Figure 2 shows the community 1 and layout of photovoltaic panels.

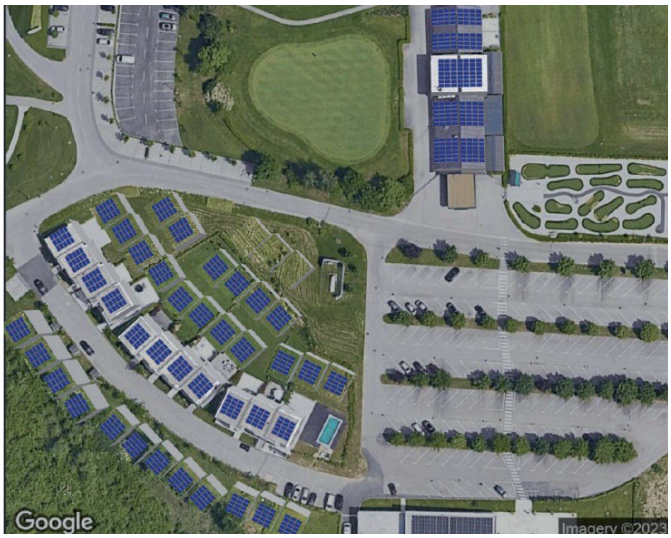

Fig. 2. Community 1

It is planned that each of the apartments consists of two bedrooms with one bathroom and a separate toilet and is 60m2 in size in order to meet the requirements of the 4-star tourist apartment categorization. The apartments and the restaurant are open all year. Restaurant and restaurant roof area data were estimated in Solar Edge software and shown in Table 1.

Table I

Areas of Buildings and Number of People in Community 1

Object	Surface area	Number of people
40 apartments/flats	2400 m²	160
Restaurant	680 m²	350
Total	3080 m²	510

There are two charging stations (Siemens VersiCharge 7.2 kW) in the parking lot, for which the estimated daily charging of two cars per charging station is 4 hours per charge. On a daily basis, the filling station consumes 115 kWh, while on an annual basis it consumes 42 MWh. The estimated annual consumption of electricity is 361.1 MWh.

Figure 3 shows energy consumption by month. The largest share of consumption for each month goes to heating and cooling.

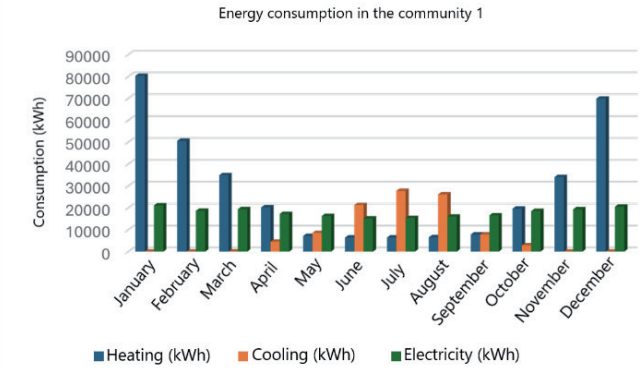

Fig. 3. Energy consumption in the community 1

The SolarEdge software tool was used to dimension production capacities. Estimated consumption and available roof area were taken into account. 209 photovoltaic panels were installed on the roof of the restaurant with an area of 680 m2, while 600 photovoltaic panels were installed on the roofs of the apartments with an area of 2,400 m², for a total of 809 photovoltaic panels. Solar Edge estimates production of 370 MWh annually. The simulated estimated annual output of Community 1 PV from Renewables ninja is 372 MWh which is slightly higher than consumption, but system operators have been more flexible in this regard over the years and the excess output should not cause problems. In the winter months consumption is significantly higher than production, while in the other months, except for the summer months, production is approximately equal to consumption or slightly higher. In the summer months, production is significantly higher than consumption, which is shown in Figure 4.

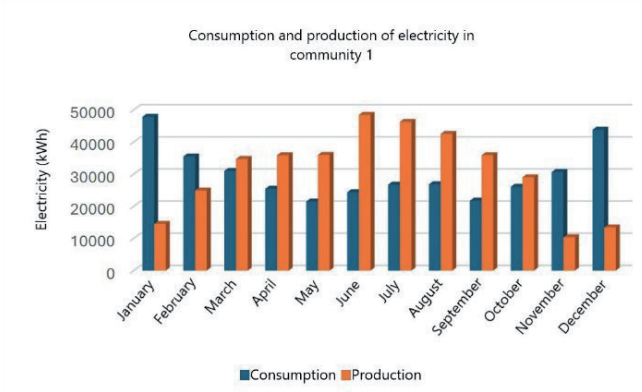

Fig. 4. Consumption and production of electricity in community 1

The average electricity consumption of the community at night is 22 kWh/hour, which for a period of 8 hours amounts to 176 kWh. The battery capacity that would enable autonomy at night is 200 kWh.

Figure 5 shows how many times per year the battery of community 1 is charged or discharged at maximum power (0.5C). In community 1, that number is 175.

Filip Dimač, Ivan Rajšl, Sara Raos and Goran Ribić , The Roles of Battery Energy Storage System in Different Energy Communities, Journal of Energy, vol. 73 Number 4 (2024), 16–25
https://doi.org/10.37798/2024734705

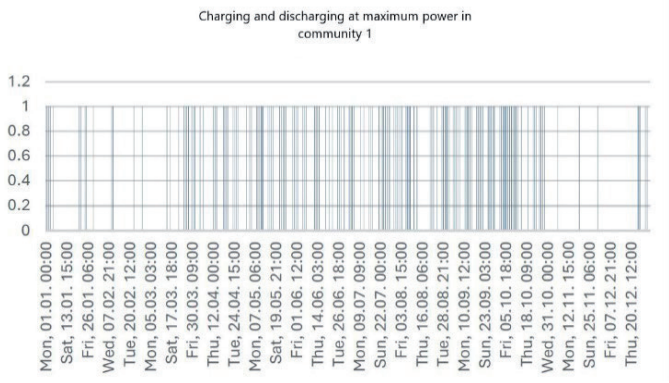

Fig. 5. Charging and discharging at maximum power in community 1

Figure 6 shows the battery activity on January 7. If you look at the activity every day of the year, by adding up the energies that entered the battery and left the battery, you can see how active the battery was. The total annual discharged energy is 78.101,97 kWh and charged energy is 78.222 kWh. If these numbers are divided by the battery capacity, it can be concluded that the battery was "discharged" 390.5 times and the battery was "charged" 391 times, which is a total of 390.5 cycles.

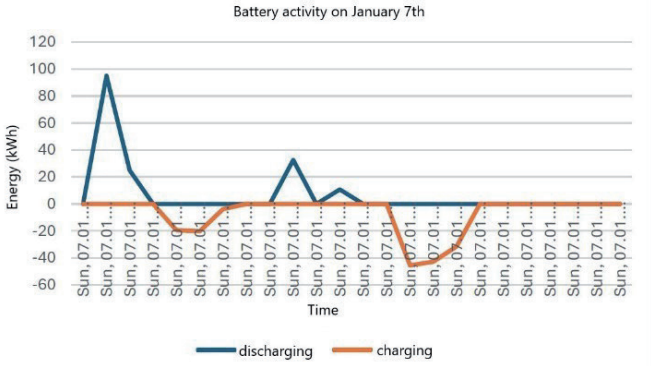

Fig. 6. Battery activity on January 7th

B. Community 2

Community 2 consists of consumption, production and BESS, and the community is located on the island of Lošinj. Consumers are: a boutique hotel and an electric vehicle charging station. Production is from photovoltaic panels that are placed on the covered parking lot and on the roof of the hotel. Figure 7 shows community 2 and the layout of the photovoltaic panels.

Although nPro software has a lot of possibilities for the purpose of precise modeling of the consumption of individual objects, there is one drawback. The consumption of community 2 differs from the others because it is seasonal in nature. It is possible to change the hourly percentages for days of the week, weekends and holidays, but it is not possible to change these data by month, that is, in the case of community 2, to model seasonal consumption, but the hotel is viewed as if it works at full capacity all year round, which is not true. For the purpose of more precise modeling of community 2, the assumption of hotel capacity occupancy is given in Table 2.

Fig. 7. – Community 2

Table II
Hotel Occupancy Capacity by Month

Month	Hotel occupancy rate [%]
January	0
February	0
March	30
April	50
May	70
June	90
July	100
August	100
September	90
October	70
November	50
December	30

In January and February, even though the hotel is not working, there is a minimum consumption of the cold operation, which is 10% of the consumption that would be in those months. Electricity consumption in the other months is scaled depending on the occupancy capacity of the hotel.

The highest turnover of the hotel, and therefore consumption, is in the summer months. The estimated annual consumption of electricity for community 2 is 422.9 MWh, which is the highest consumption of all communities. This information is not surprising considering the nature of the facility and the content it offers. Figure 8 shows the consumption of electricity by month. The largest share of consumption goes to cooling.

Filip Dimač, Ivan Rajšl, Sara Raos and Goran Ribić , The Roles of Battery Energy Storage System in Different Energy Communities, Journal of Energy, vol. 73 Number 4 (2024), 16–25
https://doi.org/10.37798/2024734705

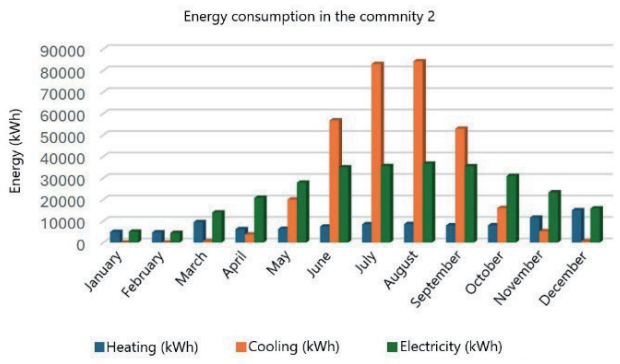

Fig. 8. Energy consumption in the community 2

The production capacities are dimensioned in such a way that the annual production is approximately equal to the annual consumption. For this purpose, 459 photovoltaic panels were installed on the roof of the covered parking lot and the hotel, facing east, west and south. The estimated annual production from the community's photovoltaic panels is 255.9 MWh. Production is significantly lower than consumption due to the lack of roof space. Electricity production in the community is highest in the summer months, and it exceeds consumption in January, February and March, while in April it is approximately equal to consumption. Display in Figure 9.

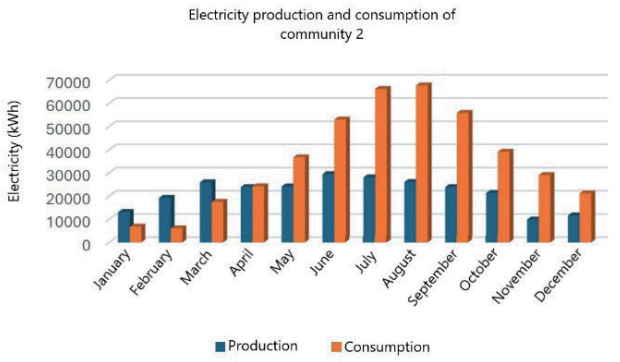

Fig. 9. Electricity production and consumption of community 2

Data on the surface of roofs and the surface of buildings were evaluated in the SolarEdge software. The hotel accommodates 160 people and employs 100 workers. Data on the area of the hotel and the number of people using the community are given in Table 3.

TABLE III

AREAS OF BUILDINGS AND NUMBER OF PEOPLE IN THE COMMUNITY 2

Object	Surface area	Number of people
Hotel	3,500 m²	260

As in Community 1, there are two charging stations for electric vehicles in the parking lot (Siemens VersiCharge 7.2 kW) which consume 42 MWh of electricity annually.

The average electricity consumption of the community at night is 32 kWh/hour, which for a period of 8 hours amounts to 256 kWh. The battery capacity that would enable autonomy at night is 300 kWh.

Figure 10 shows how many times per year the battery of community 2 is charged or discharged at maximum power (0.5C). In community 2, that number is 199. It is noticeable charging and discharging frequency 0.5C in months where production is greater or approximately equal to production.

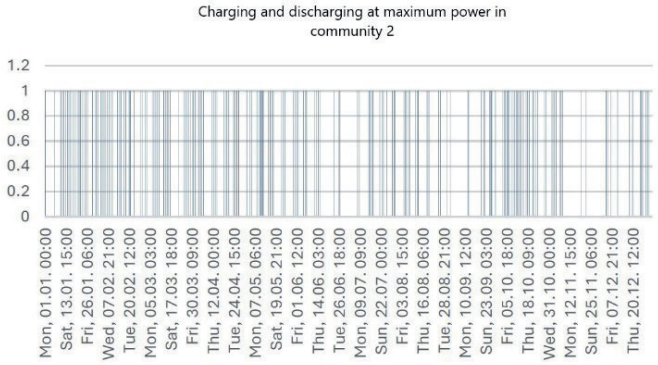

Fig. 10. Charging and discharging at maximum power in community 2

Figure 11 shows the battery activity on January 7. The total annual discharged energy is 111.647 kWh and charged energy is 111.827 kWh, which means that the battery was "discharged" 372 times while the battery was "charged" 372 times, which is a total of 372 cycles.

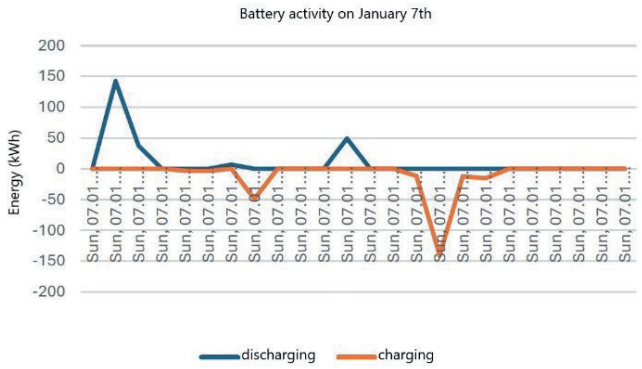

Fig. 11. Battery activity on January 7th

C. COMMUNITY 3

Community 3 includes a school, gymnasium, and kindergarten. The BESS shows significant benefits due to consistent consumption patterns. Production is from photovoltaic panels that are placed on the roof of the sports hall and elementary school. Figure 12 shows community 3.

Data on the surface of roofs and the surface of buildings were evaluated in the SolarEdge software. If an eight-year primary school has 4 classes per year and an average of 30 students per class, that amounts to 960 students. Taking into account the teachers and all other employees of the school, it was estimated that 1,000 people attend the school every day. In the kindergarten, there are 8 educational groups of 20 children per group and two kindergarten teachers per group. In addition to other employees of the kindergarten, the estimated number of people in the kindergarten every day is 190. The area of the primary school, kindergarten and sports hall and the number of people per community facility are shown in Table 4.

Filip Dimač, Ivan Rajšl, Sara Raos and Goran Ribić , The Roles of Battery Energy Storage System in Different Energy Communities, Journal of Energy, vol. 73 Number 4 (2024), 16–25
https://doi.org/10.37798/2024734705

Fig. 12. Community 3

TABLE IV

AREAS OF BUILDINGS AND NUMBER OF PEOPLE IN THE COMMUNITY 3

Object	Surface area	Number of people
Primary school	4,200 m²	1000
Kindergarten	1,250 m²	190
Sports hall	970 m²	-

The estimated annual electricity consumption for community 3 is 417 MWh.

Figure 13 shows energy consumption by month. As in every community, until now the largest share of consumption goes to heating and cooling, but in community 3 that share is significantly higher. The table shows that the highest consumption is in January, June and December. Considering the school summer holidays, it is expected that July and August are the months with the lowest consumption, along with April and September, when the needs for heating and cooling are much lower than in the summer and winter months.

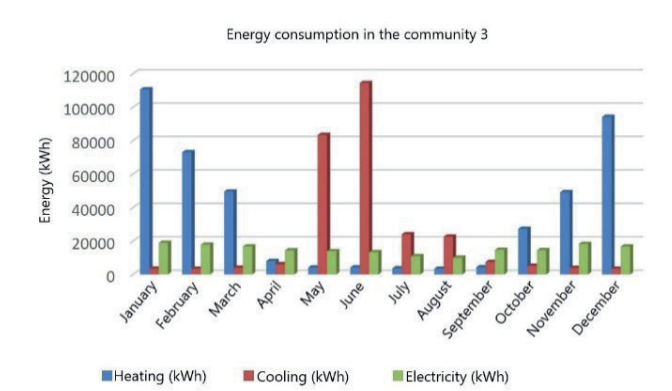

Fig. 13. – Energy consumption in the community 3

The production capacities are dimensioned in such a way that the annual production is approximately equal to the annual consumption. For this purpose, 882 photovoltaic panels were placed on the roofs of elementary schools and sports halls, facing east, west and south. According to the simulation results of SolarEdge, 392.49 kWp of DC power was installed, while the maximum achieved AC power of the power plant is 309 kW. According to the simulation, the power plant produces 443 MWh annually, Renewables.ninja-e production is somewhat different from the power plant's product 413.4 MWh. Production and consumption of the community are shown in Figure 14.

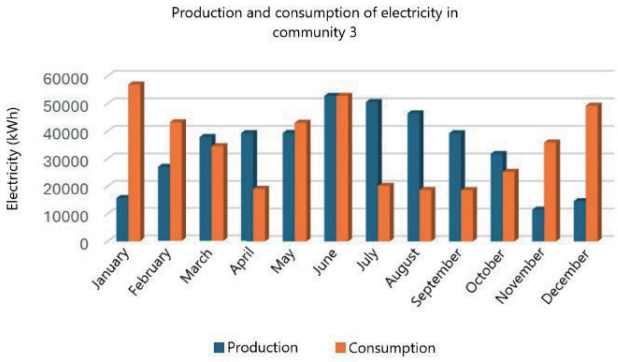

Fig. 14. Production and consumption of electricity in community 3

The average electricity consumption of the community at night is 30.4 kWh/hour, which for a period of 8 hours amounts to 243.2 kWh. Battery capacity that would enable autonomy at night is 250 kWh.

Figure 15 shows how many times per year the battery of community 3 is charged or discharged at maximum power. In community 3, that number is 171. It is noticed that the battery charges or discharges 0.5 C less often in months when consumption is higher than production.

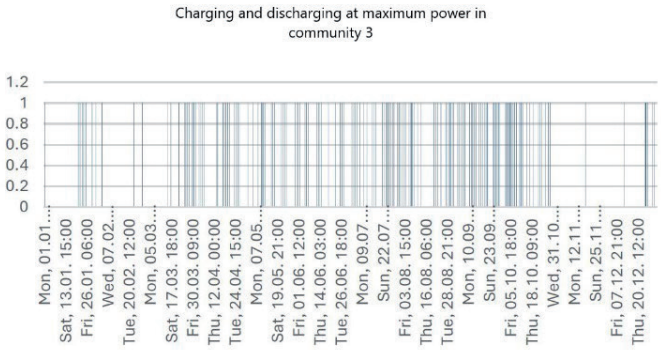

Fig. 15. Charging and discharging at maximum power in community 3

Figure 16 shows the activity of the battery on January 7. The total annual discharge energy is 96.386 kWh and charge energy is 96.536 kWh, which means that the battery "discharged" 385 times, while the battery was "charged" 386 times, which is a total of 385.5 cycles.

Filip Dimač, Ivan Rajšl, Sara Raos and Goran Ribić , The Roles of Battery Energy Storage System in Different Energy Communities, Journal of Energy, vol. 73 Number 4 (2024), 16–25
https://doi.org/10.37798/2024734705

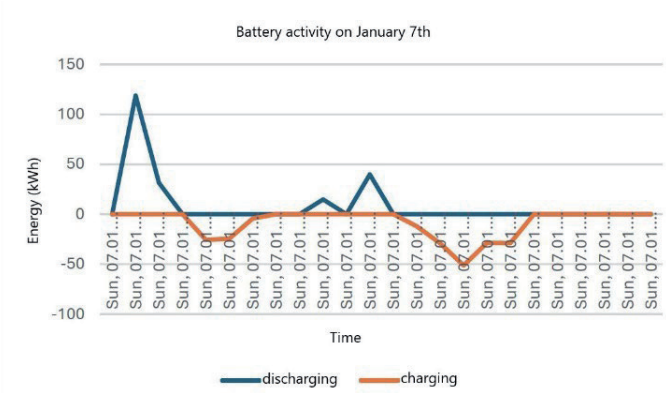

Fig. 16. Battery activity on January 7th

Figure 17 shows the battery activity for one summer day. Lower electricity prices are observed at night, but this still does not prevent the battery from doing arbitrage on the price difference and bringing profit to the community. Charging of the battery in periods of lower prices and discharge in periods of higher prices is observed.

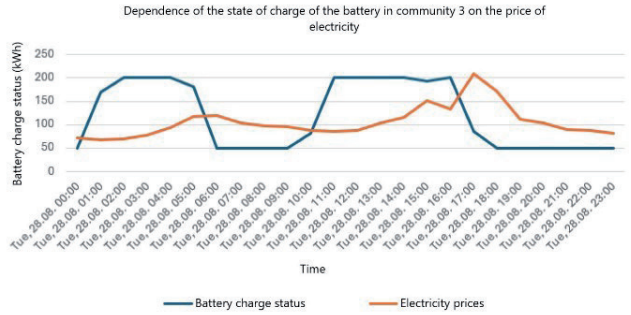

Fig. 17. Dependence of the state of charge of the battery in community 3 on the price of electricity on the date of August 28th

Figure 18 shows the activity of the battery for one winter day. There is one increase in prices per day during the period of peak consumption when citizens return home from work. During this period, the battery is discharged.

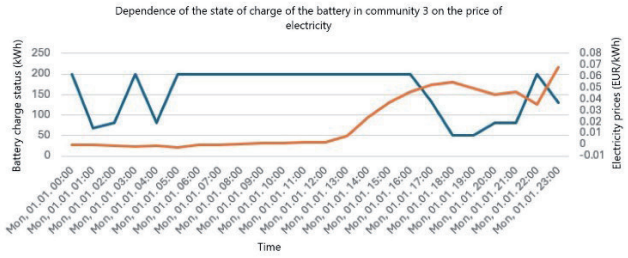

Fig. 18. - Dependence of the state of charge of the battery in community 3 on the price of electricity on the date of January 1st

D. Comparison

Tables 5, 7, 9 show investment data for each community. The investment is roughly estimated based on the costs for the solar panels and the battery, and other costs are ignored.

Tables 6, 8, 9 show annual costs and electricity savings for all communities in 4 cases. Each row in those tables is one scenario: 'Only consumption', Photovoltaic power plant, 'PV battery system with unlimited battery charging/discharging' and 'PV battery system with the condition of battery state of charge between 20% and 80%', so those tables have 4 rows with data.

The first case is when the community would be exclusively a consumer without of any production of energy or BESS. The cost of electricity for community without photovoltaic panels is calculated by adding up for each hour the hourly consumption multiple by electricity prices in that hour.

The second case is when the community would be with production from photovoltaic panels, but still without a BESS.

The third and fourth cases are for communities with the photovoltaic panels and with BESS.

In our scenario, we created 4 cases in such a way that we distinguished the differences regarding the existence or non-existence of a solar power plant and BESS, but it is possible to extend the analysis to cases in which the difference regarding the consumer itself is considered. In reference [11] authors explored such a form of scenario, but such an analysis would be useful if we wanted to elaborate in more detail on one of our 3 communities and then we would also deal with the Performance Ratio (PR) of the power plant itself, but all this represents the potential for future work and future articles.

By installing the photovoltaic panels and by installing BESS, savings are expected considering that the community is not only a consumer but also a producer who can sell their surplus energy and use the stored energy later with the BESS. Optimizing with the goal of minimal electricity costs, results were obtained in cases where the community uses a BESS.

Two cases were considered, when the full battery capacity is used and when the battery state of charge is limited between 20% and 80% of the battery capacity.

Community 1 electricity cost in case of battery charging and discharging restrictions is not significantly higher (1,300 euros per year) than the case when the battery does not have such limitations but the life of the battery is significantly extended by avoiding excessive charging and deep discharge, i.e. by maintaining a moderate level of charge, which is not a negligible factor for batteries of this capacity and their prices so it is more profitable to extend the life of the battery than to save a few thousand euros per year. The cost difference of these two cases in Community 2 is slightly higher (approximately 3,000 euros per year), but still extending battery life is more profitable. The same conclusion was reached in community 3.

Table V

Investments in the Community 1

Community 1	Number	Price per panel [EUR]	Total price [EUR]
Panels	809	200	161,800
	Capacity (kWh)	Price for 100 kWh [EUR]	
Battery	200	50,000	100,000

Filip Dimač, Ivan Rajšl, Sara Raos and Goran Ribić , The Roles of Battery Energy Storage System in Different Energy Communities, Journal of Energy, vol. 73 Number 4 (2024), 16–25
https://doi.org/10.37798/2024734705

TABLE VI

SAVINGS IN THE COMMUNITY 1

Community 1	Costs [EUR]	Saving [EUR]	Saving [EUR] per capita
Only consumption	40,340	-	-
Photovoltaic power plant	11,273	29,067	56.99
PV battery system with unlimited battery charging/discharging	4,264	36,076	70.74
PV battery system with the condition of battery state of charge between 20% and 80%	6,578	33,762	66.2

For community 1, the investment in the form of photovoltaic panels amounts to 161,800 euros and an additional 100,000 euros for the BESS. If the community 1 had only production without the possibility of storing electricity, the return on the investment is in 5.566 years (not taking into account panel degradation, inflation, accompanying costs, e.g. installation, etc.).

The return on investment for the photovoltaic panels and BESS with unlimited charge/discharge of the battery is 7.257 years (not considering battery degradation, etc.). The return on investment for the photovoltaic panels and BESS with the battery charge condition between 20% and 80% is 7.754 years.

TABLE VII

INVESTMENTS IN THE COMMUNITY 2

Community 2	Number	Price per panel [EUR]	Total price [EUR]
Panels	459	200	91,800
	Capacity (kWh)	Price for 100 kWh [EUR]	
Battery	300	50,000	150,000

TABLE VIII

SAVINGS IN THE COMMUNITY

Community 2	Costs [EUR]	Saving [EUR]	Saving [EUR] per capita
Only consumption	41,776	-	-
Photovoltaic power plant	20,585	21,191	81.5
PV battery system with unlimited battery charging/ discharging	11,365	30,411	116.97
PV battery system with the condition of battery state of charge between 20% and 80%	14,314	27,462	105.62

For community 2, the investment in the form of photovoltaic panels amounts to 91,800 euros and an additional 150,000 euros for the BESS. If the community 2 had only production without the possibility of storing electricity, the return on the investment is in 4.33 years (not taking into account panel degradation, inflation, accompanying costs, e.g. installation, etc.).

The return on investment for the photovoltaic panels and battery container with unlimited charge/discharge of the battery is 7,951 years (not considering battery degradation, etc.). The return on investment for the photovoltaic panels and BESS with the battery charge condition between 20% and 80% is 8,805 years.

TABLEIX

INVESTMENTS IN THE COMMUNITY 3

Community 3	Number	Price per panel [EUR]	Total price [EUR]
Panels	882	200	176,400
	Capacity (kWh)	Price for 100 kWh [EUR]	
Battery	250	50,000	125,000

TABLE X

SAVINGS IN THE COMMUNITY 3

Community 3	Costs [EUR]	Saving [EUR]	Saving [EUR] per capita
Only consumption	45,215	-	-
Photovoltaic power plant	12,222	32,993	27.73
PV battery system with unlimited battery charging/discharging	4,138	41,077	34.52
PV battery system with the condition of battery state of charge between 20% and 80%	6,742	38,473	32.33

For community 3, the investment in the form of photovoltaic panels amounts to 176,400 euros and an additional 125,000 euros for the BESS. If the community 3 had only production without the possibility of storing electricity, the return on the investment is in 5,347 years (not taking into account panel degradation, inflation, accompanying costs, e.g. installation, etc.).

The return on investment for the photovoltaic panels and battery container with unlimited battery charging/discharging is 7,337 years (not considering battery degradation, etc.). The return on investment for the photovoltaic panels and BESS with the battery charge condition between 20% and 80% is 7,834 years.

Table 11 shows the investment return times for all cases in all communities. The investment payback times are approximately the same for communities 1 and 3, while the investment payback time is slightly longer for community 2. Given the fact that the annual savings in community 2 are the least and that the investment payback time is the highest, i.e. less in other communities, it can be concluded that in communities 1 and 3 batteries will pay off more.

TABLE XI

INVESTMENT RETURN TIME IN COMMUNITIES

Investment return time [year]	Community 1	Community 2	Community 3
Photovoltaic power plant	5.666	4.33	5.347
PV battery system with unlimited battery charging/discharging	7.257	7.951	7.337
PV battery system with the condition of battery state of charge between 20% and 80%	7.754	8.805	7.834

Filip Dimač, Ivan Rajšl, Sara Raos and Goran Ribić , The Roles of Battery Energy Storage System in Different Energy Communities, Journal of Energy, vol. 73 Number 4 (2024), 16–25
https://doi.org/10.37798/2024734705

If, in addition to this data, the data on the activity of the battery and the way it is used are taken into account, a conclusion can be reached in which community is most profitable to install a BESS.

Table 12 shows how many times a year the battery was charged and discharged and how many times the battery was charged or discharged at 0.5 C. The number of charges and discharges at 0.5 C is observed for the reason that it is the most unfavorable way of charging and discharging the battery and thus the battery is consumed the most. Given that both numbers are smaller for community 3 than community 1, it can be concluded that battery 3 has the highest chance of having the longest life and therefore the most worthwhile.

TABLE XII

NUMBER OF BATTERY CHARGING AND DISCHARGING AND NUMBER OF 0.5C CHARGING AND DISCHARGING BY COMMUNITIES

	Community 1	Community 2	Community 3
Number of chargers and discharges (cycles) per year	390.5	372	385.5
Number of chargers and discharges at 0.5C	175	199	171
Ratio	0.2238	0.2675	0.2218

V. CONCLUSION

Energy communities offer innovative and sustainable approaches for the transformation of energy systems towards decentralisation, participation and environmental responsibility. Investments in BESS are still costly, but feasible with subsidies. Further research and technological advances are needed to make these concepts financially sustainable in the near future.

This concept promotes the local balancing of energy supply and demand, reduces greenhouse gas emissions and promotes sustainability. With the rapid development of renewable energy sources and energy storage technologies, energy communities are becoming important players in achieving energy independence and reducing dependence on traditional energy sources. The development of information and communication technologies also supports innovative management solutions in the transition from the traditional inelastic to the modern energy system.

In order to realise all the benefits of this model, it is necessary to promote it through further legal frameworks, technological innovation and education to ensure fairness, transparency and efficiency in the work of energy communities. By involving citizens in the decision-making process, creating favourable conditions for local initiatives and supporting the development of smart technologies, energy communities have the potential to become a key factor in the transition to a sustainable energy system.

Analysing the concepts of different types of energy communities explained in this paper, it can be concluded that investments in BESS are still extremely expensive, but feasible with the help of subsidies from the European Union. With further research and technological advances, these concepts will be financially feasible in the near future.

As mentioned in the introductory chapter, the high integration of photovoltaic power plants can cause the problem of overvoltage in the grid. This problem can be solved by using BESS, which are usually connected in parallel to the photovoltaic power plant. This issue is targeted as an extension and goal for future work. In addition, more attention will be focussed on virtual energy communities.

REFERENCES

[1] D. Raffaele, V. Bolwerk, L. ten Boske, I. Tjallingii, Peer to peer energy trading, Accelerating the energy transition and capturing business value value with AI and data, https://www2.deloitte.com/nl/nl/pages/energy-resources-industrials/articles/cop26-peer-to-peer-energy-trading.html. 1

[2] Directive (EU) 2019/944 of the European Parliament and of the Council of June 5, 2019 on common rules for the internal electricity market and amending Directive 2012/27/EU (amendment) 2

[3] V. Heinisch, M. Odenberger, L. Göransson, F. Johnsson, Organizing prosumers into electricity trading communities: Costs to attain electricity transfer limitations and self-sufficiency goals, Int. J. , DOI: https://doi.org/10.1002/er.4720

[4] E. Barabino, D. Fioriti, E. Guerrazzi, I. Mariuzzo, D. Poli, M. Raugi, E. Razaei, E. Schito, D. Thomopulos, Energy Communities: A review on trends, energy system modelling, business models, and optimisation objectives, Sustainable Energy, Grids and Networks, Volume 36, 2023, 101187, ISSN 2352-4677, https://doi.org/10.1016/j.segan.2023.101187

[5] coneva, Energy Communities - which models exist?, July 22,2021, https://coneva.com/en/blog/energy-communities-which-models-exist

[6] K. Berg, R. Rana, H. Farahmand, Quantifying the benefits of shared battery in a DSO-energy community cooperation, Applied Energy, Volume 343, 2023, 121105, ISSN 0306-2619, https://doi.org/10.1016/j.apenergy.2023.121105.

[7] EMBER, European wholesale electricity price data, 1.4.2024, https://ember-climate.org/data-catalogue/european-wholesale-electricity-price-data/

[8] KSTAR, https://www.kstar.com/EnergyStorageInverter/19257.jhtml, 28.12.2023.

[9] Ivan Pavić, Tomislav Capuder, Igor Kuzle: Generation scheduling in power systems with high penetration of renewable energy, Journal of Energy, Volume 66, Number 1-4 (2017), Special Issue Selected graduation thesis, DOI: https://doi.org/10.37798/2017661-4102

[10] Goran Grdenić, Željko Tomšić: Renewable energy sources and other energy technologies as a measure for mitigating the impact of urban heat islands, Journal of Energy, Volume 66, Number 1-4 (2017), Special Issue Selected graduation thesis, DOI: https://doi.org/10.37798/2017661-4104

[11] Saleh Eshtaiwi, Mustafa Aburwais, Mustafa Elayeb, Mohamed Abozaed, Mohamed Shetwan: The Impact of Residential Optimally Designed Rooftop PV System on Libya Power Shortage Case, Journal of Energy, Volume 71, Number 3 (2022), Energija (03/2022), DOI: https://doi.org/10.37798/2022713377

[12] Laszlo Horvath, Danijel Beljan, Andrea Marić, Miroslav Elezović: Power Variability of Wind and Solar Production Portfolio in the Republic of Croatia, Journal of Energy, Volume 71, Number 2 (2022), Energija (02/2022), DOI: https://doi.org/10.37798/2022712408

[13] Gurobi Optimization, LLC (2024). Gurobi Optimizer Reference Manual. Retrieved from https://www.gurobi.com

[14] SolarEdge Technologies, Inc. (n.d.). SolarEdge Designer [Software]. Retrieved from https://www.solaredge.com/products/software-tools/designer

[15] Pfenninger, Stefan and Staffell, Iain (2016). Long-term patterns of European PV output using 30 years of validated hourly reanalysis and satellite data. Energy 114, pp. 1251-1265. doi: 10.1016/j.energy.2016.08.060, https://www.renewables.ninja/

[16] Staffell, Iain and Pfenninger, Stefan (2016). Using Bias-Corrected Reanalysis to Simulate Current and Future Wind Power Output. Energy 114, pp. 1224-1239.doi:10.1016/j.energy.2016.08.068,https://www.renewables.ninja/

Filip Dimač, Ivan Rajšl, Sara Raos and Goran Ribić , The Roles of Battery Energy Storage System in Different Energy Communities, Journal of Energy, vol. 73 Number 4 (2024), 16–25
https://doi.org/10.37798/2024734705

Journal of Energy

VOLUME 73 Number 4 | 2024

journal homepage: http://journalofenergy.com/

Regional Solar Irradiance Forecasting Using Multi-Camera Sky Imagery and Machine Learning Models

Alen Jakoplić, Dubravko Franković, Tomislav Plavšić, Branka Dobraš

***Summary* — With the increasing integration of photovoltaic (PV) systems into power grids, accurate short-term solar irradiance forecasting is essential for efficient energy management. This paper presents a machine learning model developed using a synthetic dataset designed to analyze the potential of multicamera sky imaging for regional solar irradiance forecasting. The dataset, generated in a controlled simulation environment, captures cloud dynamics and solar irradiance at multiple locations within a region. The proposed model utilizes sky images from multiple virtual cameras strategically positioned to provide spatially distributed observations. By combining image-based features with historical irradiance measurements, the model shows improved forecasting accuracy compared to single-camera approaches. The results indicate that multi-camera systems better capture the spatial variability of cloud cover and allow the model to predict solar irradiance for locations without installed cameras. This research highlights the potential of multi-camera configurations for regional forecasting and provides valuable insights for grid operators and energy planners. The results support the adoption of distributed sky imaging networks as a practical approach to improve solar irradiance predictions and ultimately contribute to the stability and reliability of solarpowered energy systems through improved forecast accuracy.**

***Keywords* — Solar irradiance forecasting, photovoltaic systems, multi-camera sky imaging, renewable energy integration.**

I. Introduction

Photovoltaic power plants (PVPPs) are among the most widely used renewable energy power plants [1]. Their popularity stems from their ability to harness solar energy, an abundant and inexhaustible resource while generating electricity with minimal environmental impact. Due to their lower environmental impact, research has recently focused on further improving solar cells in terms of efficiency, production costs, and durability. The constant advances in photovoltaic technology have led to higher efficiency, longer lifespan, and lower manufacturing costs, which have accelerated the use of PV systems worldwide. As a result, the share of PVPPs in the structure of production units in the energy sector is steadily increasing, making solar energy a cornerstone of the transition to cleaner energy systems [2].

The unpredictability of electricity generation from renewable energy sources, including solar energy, leads to voltage and frequency fluctuations within the power grid, causing difficulties in its management [3]. These fluctuations are caused by sudden changes in solar radiation due to cloud movements, atmospheric conditions, and other meteorological factors. Changes in the availability of renewable energy can occur within very short periods, often only a few minutes, during which other, conventional power plants cannot adjust their output quickly enough. The inherently slow response of conventional power plants, such as coal or gas-fired power plants, exacerbates the imbalance between electricity generation and consumer demand. When the balance between generated and consumed electricity is disturbed, deviations from nominal voltage and frequency values occur, resulting in reduced quality of electrical energy and potential damage to sensitive equipment [4], [5].

To mitigate the negative impact of renewable energy sources on the power grid, it is necessary to predict changes in the availability of these energy sources with a certain degree of accuracy. The highly dynamic nature of meteorological conditions makes accurate long-term cloud forecasting at a given location difficult [6]. Conventional meteorological models, while effective at larger scales, are often inadequate when applied to local cloud dynamics relevant to PV power prediction. A promising solution to this challenge is the short-term prediction of cloud cover at the observed location, typically 10 to 15 minutes in advance within a radius of 2000 meters. Narrow spatial and temporal scales enable more accurate prediction of cloud cover and thus better integration of solar energy into the grid and more effective planning of the operation of conventional power plants [7].

Implementing a reliable power generation forecasting system reduces the need for balancing power, i.e. the reserve power needed to compensate for deviations of renewable energy generation from the contracted schedule. More accurate forecasts consequently reduce the cost of integrating renewable energy sources into the electricity grid by minimizing the dependence on reserve power plants and ancillary services [8]. In addition, the reduction of production curtailments due to large fluctuations leads to higher efficiency of existing systems. This improved efficiency combined with lower integration costs not only benefits grid operators but also leads to lower electricity prices for consumers within the grid. In addition, improved forecasting capabilities support grid stability, reliability, and resilience, especially as the share of variable renewable energy sources continues to increase in modern power systems [9].

(Corresponding author: Alen Jakoplić)

Alen Jakoplić, Dubravko Franković, and Branka Dobraš are with the Faculty of Engineering, University of Rijeka, Rijeka, Croatia (e-mails: alen.jakoplic@riteh.uniri.hr, dubravko.frankovic@riteh.uniri.hr, branka.dobras@riteh.uniri.hr)

Tomislav Plavšić is with the Croatian Transmission System Operator (HOPS), Zagreb, Croatia (e-mail: tomislav.plavsic@hops.hr)

Alen Jakoplić, Dubravko Franković, Tomislav Plavšić, Branka Dobraš, Regional Solar Irradiance Forecasting Using Multi-Camera Sky Imagery and Machine Learning Models, Journal of Energy, vol. 73 Number 4 (2024), 26–33
https://doi.org/10.37798/2024734707

Building on the existing foundation, this research focuses on the development of a short-term prediction model for solar radiation using a synthetic database. The main objective is to investigate the potential of using multiple sky cameras at different locations to predict solar irradiance on a regional scale. By using data from multiple cameras, the model can detect cloud patterns, movements, and shadow propagation, all of which have a significant impact on the production of photovoltaic power plants. The use of multiple cameras provides the model with a more comprehensive understanding of atmospheric dynamics, as the combination of different viewing angles enables better recognition of cloud formation and movement trends.

The ability to forecast solar radiation regionally offers several advantages. It enables predictions for areas where no cameras are directly installed, extending the practical applications of the model beyond the monitored locations. This is particularly valuable for distributed PV systems, where individual installations may be spread over a larger geographical area. In addition, improved short-term forecasting supports better grid management, as operators can anticipate fluctuations in solar power generation and implement necessary balancing measures more effectively.

Ultimately, this study shows that it is possible to use multicamera configurations to improve short-term solar irradiance forecasting at a regional level. The knowledge gained from this study contributes to ongoing efforts to improve the integration of renewable energy sources into modern power systems and to support a more stable, efficient, and reliable use of solar energy.

II. Basics and Motivation for Regional Solar Forecasting Models

In recent years, with significant integration of PV power plants, mostly at lower voltage levels, accurate solar irradiance forecasting is becoming crucial for stable and secure power system operation. Solar irradiance forecasting is an input variable for two important power system operational planning processes:

- PV production forecasting
- Load forecasting

While direct PV production forecasting is mainly used for PV power plants connected to the transmission voltage levels, load forecasting algorithms have an indirect forecast of PV generation connected to the distribution voltage levels embedded as a part of the overall forecasting function. While the load forecasting function is usually only performed as part of day-ahead operational planning processes, the forecast of renewable energy production is also performed in intra–day operational planning processes, usually one hour ahead. Such an approach is justified due to the sudden changes in local weather forecasts, which can have a significant impact on the production of PV and wind power plants. Ultrashortterm PV production forecasting 15 minutes ahead of real-time could further improve the power system operation efficiency and security, enabling the operators in control centers to take the necessary preventive operational measures just ahead of real-time. This way, the operating personnel still have time to optimize power system operation, while if those measures were curative and done after the changes in the PV production have occurred, there would be much less room for optimized operational actions.

Over the years, a large number of different methods and approaches have been developed to predict the production of PV systems [10]. These methods have evolved significantly due to the growing need for more accurate and reliable predictions to optimize grid operations and support the increasing share of solar energy in modern power systems. The categorization of these methods is generally based on the type of input data, approaches to data pre-processing, temporal frequency of data collection, spatial resolution, and temporal and spatial horizon [11]. In addition, factors such as the complexity of the model, the computational requirements, and the availability of historical data play a crucial role in determining the effectiveness of these forecasting methods.

An important aspect of forecasting the production of photovoltaic power plants lies in the analysis of local weather conditions, especially solar radiation, whose fluctuations directly affect the output power and allow an accurate prediction of future production. Solar radiation is the main factor influencing photovoltaic output, and its fluctuations are influenced by various atmospheric phenomena such as cloud cover, aerosols, and seasonal changes. Parameters such as wind speed, temperature, time of day, and relative humidity, on the other hand, have a much lower correlation with the production of photovoltaic systems. While these meteorological variables are useful for broader climatological analyses, they are often less relevant for short-term predictions. Such data are often subject to fluctuations due to various conditions, such as changes in wind direction and speed at different heights above the ground and the relative stability of temperature over a short period within a day [12]. Therefore, these parameters often require more complex models and algorithms for effective inclusion in forecasting models.

The importance of short-term prediction of solar irradiance cannot be neglected when it comes to predicting the output power of photovoltaic power plants. This type of prediction is particularly important during periods of high solar variability, e.g. on partly cloudy days, when rapid changes in irradiance can lead to significant fluctuations in PV output. The complexity of this task lies in the inherent randomness and non-linearity of solar radiation, which is particularly pronounced in changing weather conditions. Many scientific studies have emphasized the use of artificial neural networks (ANN) for such forecasting models due to their ability to adapt to complex and nonlinear patterns [13], [14]. These models use historical and real-time data to learn the intricate relationships between atmospheric conditions and solar radiation. Nevertheless, further refinement of these models in terms of accuracy and robustness is needed [15], especially in scenarios with highly dynamic cloud formations.

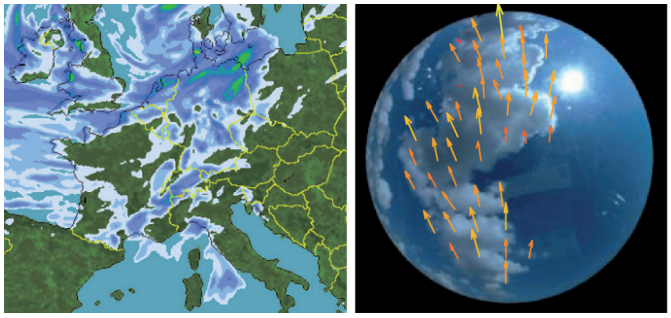

Fig. 1. Comparison of satellite and ground-based cloud motion vectors.

Forecasts of the output power of photovoltaic power plants are often based on satellite images and use models such as cloud motion vectors, as can be seen in Figure 1 on the left and right. These methods use historical cloud movement data to predict future irradiance patterns. However, the limitations of these models, such as the assumption of constant cloud shapes and sensitivity to local weather conditions, make them less accurate [16]. While satellite images are beneficial for large-scale analyses, they often lack the spatial and temporal resolution needed for accurate short-term predictions.

Accurate prediction of cloud changes over PVPPs requires detailed data on the state of clouds, including their amount, position,

Alen Jakoplić, Dubravko Franković, Tomislav Plavšić, Branka Dobraš, Regional Solar Irradiance Forecasting Using Multi-Camera Sky Imagery and Machine Learning Models, Journal of Energy, vol. 73 Number 4 (2024), 26–33
https://doi.org/10.37798/2024734707

and movement, which are usually obtained from satellite and radar imagery [17]. However, due to the limited temporal and spatial resolution of these images, they are often not suitable for short-term predictions [18]. Ground-based sky cameras equipped with wide-angle lenses and high-frequency imaging offer a promising alternative for capturing cloud dynamics in real-time. The development of new databases containing more detailed information from sky photography can significantly improve the accuracy of predictions, but high equipment costs limit their application [19], [20].

Convolutional neural networks (CNNs) are particularly well suited for detecting nonlinear relationships between input and output data in models for short-term prediction of photovoltaic power plant production. CNNs excel at processing visual information and can automatically extract relevant features from sky images without manual intervention. These networks can recognize patterns in photographs so that they can use these images as input data. Since photographs of the sky above a photovoltaic power plant are directly correlated with its output [21], convolutional neural networks can use these photographs to discover correlations between sky images and the output of photovoltaic power plants. By incorporating additional meteorological data, CNNs can achieve even higher forecasting accuracy, especially for short-term forecasts.

Based on the review of the available methods, it is concluded that the accuracy of the models generated by convolutional neural networks depends on the quality of the input data. The availability of high-quality sky images in combination with precise irradiance measurements plays a crucial role in the training and validation of the models. This underlines the importance of a detailed and comprehensive database that would enable better training of the neural network and thus a more accurate prediction of the production of photovoltaic power plants.

The development of specialized databases for short-term regional solar forecasting is essential for testing and validating new model architectures. General or single-camera datasets often fail to capture the spatial variability of cloud cover over larger areas, which is critical for understanding cloud dynamics and their impact on photovoltaic production. A customized dataset that accounts for different weather conditions and spatial configurations provides the necessary basis for improving model performance and exploring novel approaches for regional solar irradiance forecasting.

III. Development 0f a Multi-Camera Solar Forecasting Model

The development of a reliable model for short-term solar irradiance forecasting at a regional level requires an innovative approach that takes into account the complex interactions between atmospheric conditions and solar irradiance. In this study, a synthetic database with data from multiple wideangle cameras is used to capture cloud movements and their effects on solar radiation. This method enables the creation of models capable of predicting solar irradiance for locations without direct measurements by utilizing spatial relationships and cloud dynamics.

A. Synthetic Data Set Simulation Framework

The synthetic data base used in this study was created using the Unity development platform, which was chosen for its flexibility in generating realistic atmospheric scenarios and simulating dynamic cloud behavior. Unity's advanced 3D rendering capabilities and real-time simulation tools enable the accurate reproduction of sunlight behavior and cloud patterns under different weather conditions.

To ensure the fidelity of the simulations, the High Definition Render Pipeline (HDRP) was used. HDRP supports realistic light interactions, which is essential for modeling variations in solar radiation due to cloud cover, as can be seen in Figure 2. The simulation framework consists of several userdefined scripts that control environmental parameters such as sun position, cloud density, cloud movement, and temporal progression to replicate diurnal cycles.

Camera placement is calculated to cover key areas within the simulation. A script assigns coordinates to each camera, providing a variety of perspectives in the monitored region. The cameras capture sky images at regular intervals, providing a continuous stream of visual data that is essential for training the forecasting model. The image resolution is set to 64x64 efficiency. However, the framework allows customization for higher resolutions.

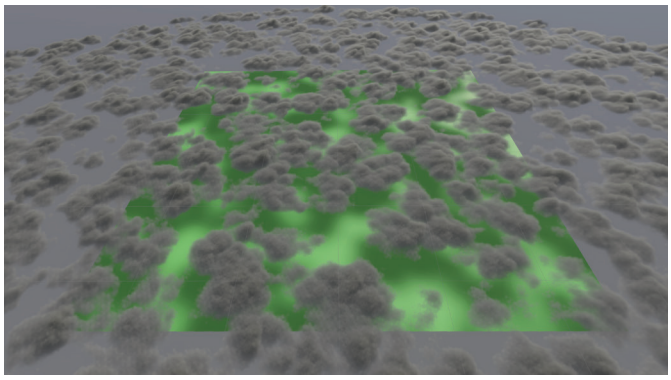

Fig. 2. Simulated cloud coverage over the target region generated using the Unity HDRP framework. The image illustrates the spatial distribution of clouds and the resulting shadows cast on the ground. The observed area is represented by the green square in the center, corresponding to a simulated surface of 50 × 50 kilometers.

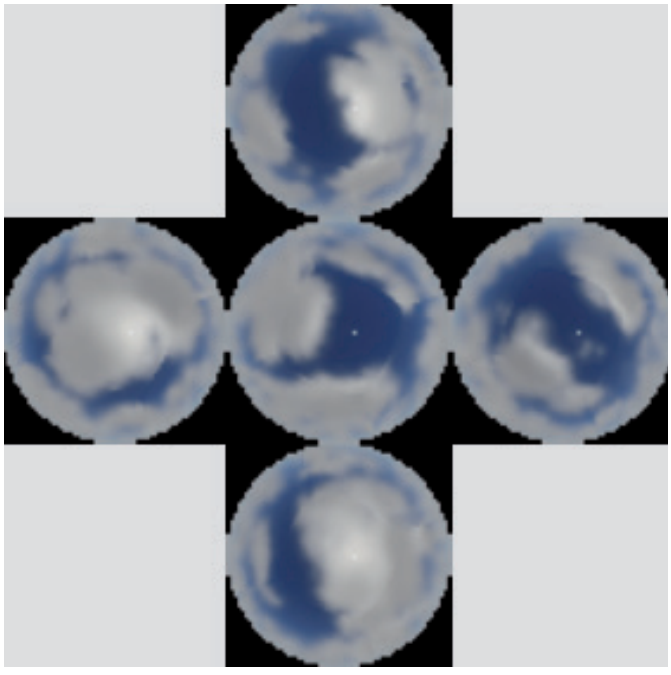

Fig. 3. Sky Images from Different Perspectives: Central Camera (0,0) with Surrounding Cameras at (-5000,0), (5000,0), (0,5000), and (0,-5000).

The simulation process was tested on an M3 MacBook Air generating a single day's data from five camera positions with images taken every five minutes took about two minutes. The resulting data set requires 8.1 MB of disk space, which underlines the scalability of the system for larger simulations. The temporal resolution

Alen Jakoplić, Dubravko Franković, Tomislav Plavšić, Branka Dobraš, Regional Solar Irradiance Forecasting Using Multi-Camera Sky Imagery and Machine Learning Models, Journal of Energy, vol. 73 Number 4 (2024), 26–33
https://doi.org/10.37798/2024734707

is set to five minutes and provides sufficient data granularity for short-term forecast models. Shorter intervals, e.g. one minute, can be configured if required to capture rapid changes in cloud cover.

The simulated area spans 50 x 50 km, with cameras strategically placed in the center and four surrounding cameras placed 5 km away in different directions to capture different cloud perspectives, as shown in Figure 3. Each camera is accompanied by light sensors that provide reference irradiance measurements to ensure that the image features match the irradiance data.

The database is publicly accessible via the Kaggle platform [22], facilitating data sharing and collaboration between researchers. The published dataset contains extensive metadata and a total size of 5.1 GB, providing a rich resource for model training and validation.

This simulation framework forms the basis for the development of advanced models for short-term solar irradiance forecasting. By incorporating multiple perspectives and different weather conditions, the model can more accurately predict cloud-related variations in solar irradiance, supporting more reliable and efficient photovoltaic power generation on a regional scale.

B. Architecture Of The Neural Network

The development and training of the neural network model for the short-term prediction of solar irradiance was performed with Google Colab, using an L4 GPU for efficient parallel processing. Google Colab provides a cloud-based environment that simplifies access to computational resources without the need for extensive local infrastructure. This platform was chosen for its flexibility, ease of collaboration, and support for GPU-accelerated machine learning workflows.

The synthetic dataset used to train the model includes 340 days of data, with measurements taken every five minutes between 6:00 am and 6:00 pm. For each of the five simulated camera locations, the database contains hemispheric sky images together with corresponding measurements of available solar radiation. This setup provides a diverse and dynamic dataset that reflects varying meteorological conditions on different days and at different times. As illustrated in Figure 4, the solar irradiance levels for five different locations are shown for two randomly selected days, providing insight into the temporal variations in solar radiation under different meteorological conditions.

Prior to training, the data was pre-processed to improve the performance of the model. The pre-processing steps included normalizing the irradiance values and temporal features to standardize the input distribution. Normalization is crucial to accelerate the convergence of the model and improve the stability of the training by ensuring that the input features have similar scales.

A custom sequence generator was implemented to prepare the data for training. This generator creates sequences of nine consecutive images for each camera, with corresponding irradiance measurements, timestamps, and camera coordinates. Each sequence represents a 45-minute time window selected based on the observed average time for cloud movement from the edge to the center of the sky image. The target value for the prediction is the irradiance at the center position (0.0) 15 minutes in the future, which corresponds to the third image ahead of the input sequence.

The decision to use a 45-minute input sequence with a 15-minute forecast horizon was guided by the dynamic characteristics of cloud movement within the synthetic data set. In the simulations, wind speeds vary daily and throughout the day. However, the 45-minute window has been shown to capture the predominant cloud movement patterns and allows the model to learn the relationship between cloud dynamics and solar irradiance variations.

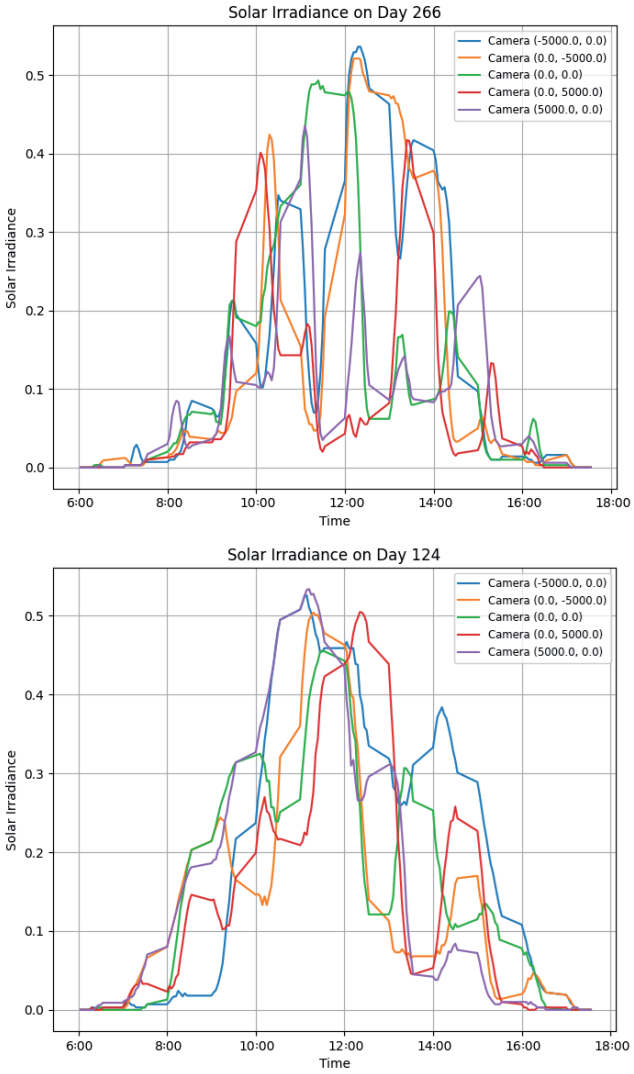

Fig. 4. Measured solar irradiance at five simulated locations on Day 266 (top) and Day 124 (bottom). Each curve represents irradiance values recorded by a dedicated irradiance module colocated with one of the five virtual sky cameras positioned at coordinates (0, 0), (±5000, 0), and (0, ±5000).

The selection of these parameters was aimed at enabling a meaningful performance analysis. Future research using real data, which is currently unavailable due to a lack of databases of sky images from multiple locations, will investigate the optimal length of input sequences and forecast horizons for regional solar forecasting.

The neural network model developed for this study was designed for short-term solar irradiance forecasting using data from multiple sky cameras together with numerical weather information. The architecture integrates convolutional neural networks (CNNs) for image processing and fully connected layers for numerical data, allowing the model to capture spatial cloud patterns and their relationship to solar radiation.

As illustrated in Figure 5, the model accepts two different inputs: The first input consists of time-sequenced images from five cameras, one central reference camera, and four peripheral cameras positioned around it. These images capture cloud movements and atmospheric conditions that influence solar irradiance. The second input comprises the corresponding meteorological param-

Alen Jakoplić, Dubravko Franković, Tomislav Plavšić, Branka Dobraš, Regional Solar Irradiance Forecasting Using Multi-Camera Sky Imagery and Machine Learning Models, Journal of Energy, vol. 73 Number 4 (2024), 26–33
https://doi.org/10.37798/2024734707

eters, such as irradiance and cloud-related features, for the same time intervals.

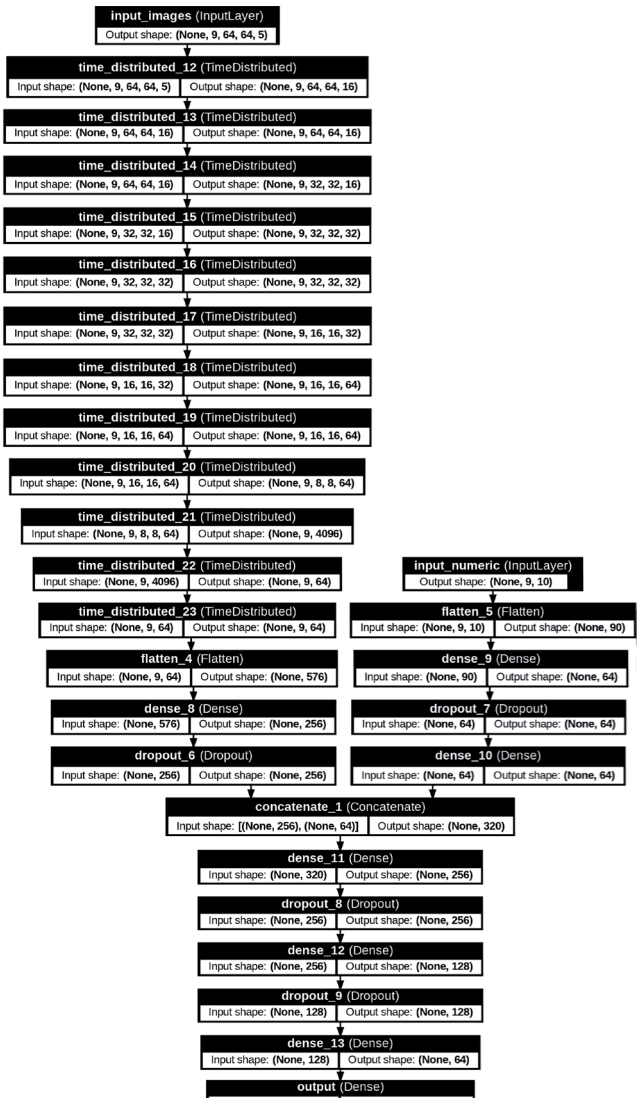

Fig. 5. Neural network architecture for regional solar forecasting.

The image processing branch uses a TimeDistributed Convolutional Neural Network (CNN) to extract spatial features from the sky images over the nine time steps. The network consists of:

- A series of three convolutional layers with filter sizes of 16, 32, and 64, each using a 3x3 kernel and ReLU activation
- Batch normalization layers after each convolutional layer
- Max-pooling layers to reduce spatial dimensions and retain essential features
- TimeDistributed flattening and dense layers to capture temporal dependencies
- A final dense layer with 256 units to combine the extracted features across all time steps

The numerical data stream processes a feature set consisting of the capture time and coordinates for each camera. This data stream passes through:

- An initial flattening layer
- Two dense layers with 64 units each and ReLU activation
- Dropout layers with a dropout rate of 20 to prevent overfitting

The outputs of the two branches are concatenated into a combined feature vector that is further processed by:

- A dense layer with 256 units and ReLU activation
- A dropout layer with a dropout rate of 30
- Additional dense layers with 128 and 64 units
- A final dense layer with a linear activation function to predict the future solar irradiance value

The model was compiled with the Adam optimizer, mean squared error (MSE) as the loss function, and a custom R^2 metric for performance evaluation. The training was performed with a batch size of 32 over 50 epochs.

The dataset was split into training (80%), validation (10%), and test subsets (10%). During training, the model was exposed to a diverse range of cloud patterns and atmospheric conditions to improve its predictive capabilities for unseen data.

To improve generalization and prevent overfitting, the training process employed early stopping with a patience of 10 epochs and model checkpointing, ensuring the retention of the best-performing model based on validation loss. The model includes a total of 566,097 trainable parameters.

Figure 6 shows the training and validation loss curves along with the validation R2 score throughout the 50 training epochs for scenario c) Camera-Free Target Location. The plot indicates stable convergence of the training loss, while fluctuations in the validation R2 metric reflect the challenging nature of the scenario, where no direct camera data from the target location is available.

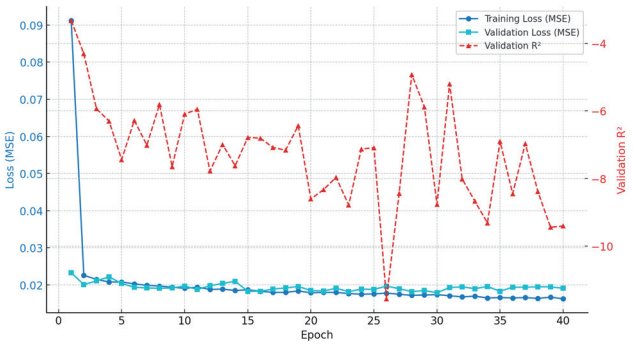

Fig. 6. Training and validation loss (MSE) and validation R2 score per epoch for scenario c) Camera-Free Target Location.

IV. Analysis of Model Accuracy in Regional Solar Forecasting

To evaluate the performance and feasibility of the developed model for regional solar forecasting, three different scenarios were designed, as illustrated in Figure 7. Each scenario explores different configurations of camera input data to evaluate the impact of different perspectives on forecasting accuracy and to investigate the potential of predicting solar irradiance for unmonitored locations.

In the first scenario (see Figure 7a), the model uses only the data from the central camera positioned at coordinates (0,0) to predict future solar irradiance at the same location. This scenario serves as a reference point against which the performance of the other scenarios can be compared. Since only a single camera is used, the model relies solely on the cloud movement patterns observed from this single viewpoint.

The second scenario (see Figure 7b) adds additional information by including the images from the four peripheral cameras at (5000,0), (-5000,0), (0,5000), and (0,-5000) meters in addition to

Alen Jakoplić, Dubravko Franković, Tomislav Plavšić, Branka Dobraš, Regional Solar Irradiance Forecasting Using Multi-Camera Sky Imagery and Machine Learning Models, Journal of Energy, vol. 73 Number 4 (2024), 26–33
https://doi.org/10.37798/2024734707

the data from the central camera. This configuration aims to determine whether the inclusion of multiple viewpoints can improve prediction accuracy. The peripheral cameras provide spatial context by capturing cloud motion from multiple vantage points, allowing the model to better understand the dynamics of cloud formation, breakup, and movement in the region.

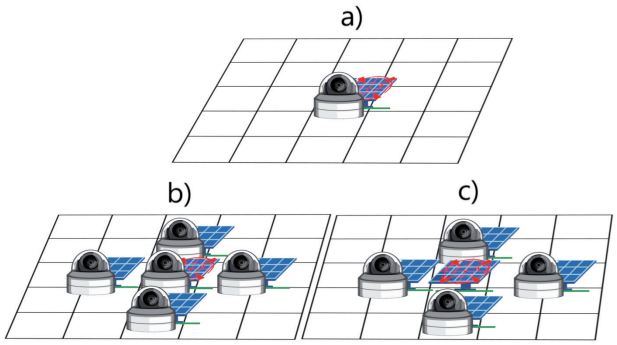

Fig. 7. Evaluation scenarios for model performance. a) Single-Camera Scenario, b) Multi-Camera Scenario, c) Camera-Free Target Location.

In the third and final scenario (see Figure 7c), the model uses only the data from the four peripheral cameras to predict solar irradiance at the central location (0,0). This scenario is particularly important as it tests the model's ability to estimate solar irradiance for a location where there is no direct monitoring device. The success of this approach would show that the model can provide forecasts for locations without installed cameras and thus support solar forecasting on a regional scale.

The performance in these three scenarios provides insight into the benefits of using multiple cameras for short-term solar irradiance prediction. It also evaluates the model's ability to generalize spatial relationships between cloud structures and irradiance patterns, providing valuable information for optimizing the placement of cameras in real-world applications.

Figures 8, 9 and 10 show the results of the solar radiation forecasts for all three evaluation scenarios. Each figure compares the actual irradiance available at the target location with the values predicted by the model. These visualizations provide a clear understanding of how the model performs under different input configurations and illustrate the impact of including multiple cameras on prediction accuracy.

The results show that the model performs satisfactorily in all three scenarios and effectively captures the relationship between cloud motion and solar irradiance variations. However, the differences in the performance metrics reveal the additional benefits of using multiple camera perspectives.

In the single-camera scenario (Scenario A), using only the data from the central camera, the model achieved a R2 score of 0.85. This scenario, illustrated in Figure 8, serves as a baseline for comparison and indicates that the model is capable of learning and predicting irradiation patterns to a reasonable extent even with a single camera. However, the limitations of using only one camera are obvious, as it provides a limited perspective on cloud motion. Without additional viewpoints, the model lacks a comprehensive spatial context, leading to occasional discrepancies between the predicted and actual values.

In contrast, the multi-camera scenario (Scenario B), which includes the images from all five cameras, significantly improves the prediction accuracy and leads to a R2 score of 0.87 as shown in Figure 9. The additional spatial context provided by the peripheral cameras allows the model to better understand cloud dynamics, shadow propagation, and irradiance variations. This improvement demonstrates the benefit of multi-camera configurations as they allow the model to generalize more effectively across different weather conditions and improve short-term forecasting capabilities.

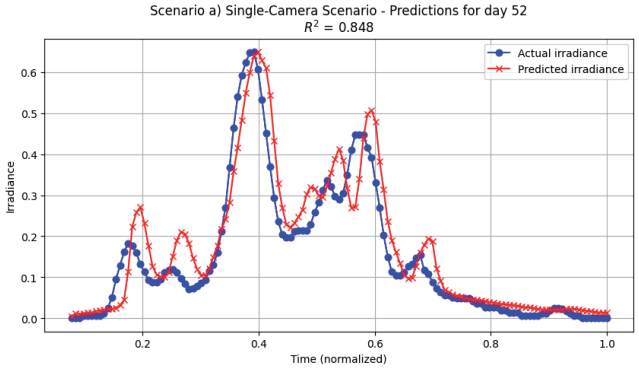

Fig. 8. Predicted and actual solar irradiance values for the single-camera cenario (Scenario A) on Day 52. Only data from the central camera at position (0, 0) were used for prediction.

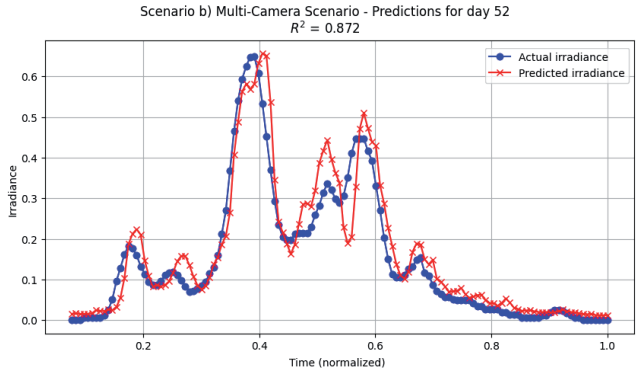

Fig. 9. Predicted and actual solar irradiance values for the multi-camera scenario (Scenario B) on Day 52. The model utilizes image data from five spatially distributed cameras to generate predictions.

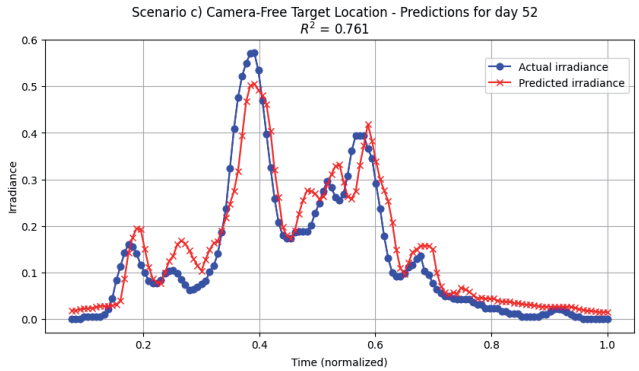

Fig. 10. Predicted and actual solar irradiance values for the camera-free target location scenario (Scenario C) on Day 52. In this setup, the model predicts irradiance at the central location (0, 0) using only images from the four peripheral cameras.

The most critical test is the camera-free target location scenario (Scenario C), where the model predicts solar irradiance at the central location without using direct images from that point. In this case, the model relies solely on the four peripheral cameras to determine the irradiance at the target location. Despite the absence of a direct monitoring device, the model still achieves a

Alen Jakoplić, Dubravko Franković, Tomislav Plavšić, Branka Dobraš, Regional Solar Irradiance Forecasting Using Multi-Camera Sky Imagery and Machine Learning Models, Journal of Energy, vol. 73 Number 4 (2024), 26–33
https://doi.org/10.37798/2024734707

R2 score of 0.76 as is evident from Figure 10., confirming that spatially distributed observations can successfully estimate irradiance for unmonitored areas. Although the performance is slightly lower compared to Scenario A and Scenario B, the results indicate that regional solar forecasting is feasible even if cameras are not installed at every location of interest.

Table I summarizes the R2 performance metrics for all three scenarios shown in Figures 8–10. The single-camera scenario (a) serves as a baseline, while the multi-camera configuration (b) shows improved accuracy due to spatially enriched input. The third scenario (c) still achieves satisfactory prediction performance despite the exclusive use of peripheral cameras, which supports the applicability of the model in cases where direct sky images of the target location are not available.

TABLE I

PREDICTION PERFORMANCE ACROSS DIFFERENT FORECASTING SCENARIOS.

Scenario	Description	R^2 Score
a) Single-Camera Scenario	Only central camera	0.848
b) Multi-Camera Scenario	Central + four peripheral cameras	0.872
c) Camera-Free Target Location	Only four peripheral cameras	0.761

It is important to recognize the limitations associated with using a purely synthetic dataset for this study. While the Unity simulation framework allows for controlled experiments and rapid generation of different scenarios, it inevitably simplifies the complexity of real atmospheric physics. Factors such as unpredictable, rapid weather changes beyond the simulated patterns, variations in aerosol concentration, subtle cloud formations (e.g. thin cirrus clouds), and potential sensor noise or calibration issues with physical cameras are not fully captured by the current synthetic data. While the presented results show the potential and feasibility of the multi-camera approach for regional forecasting, the achieved performance metrics (R2 values) should be interpreted as an upper-bound estimate under idealized conditions. Future work will focus on the validation of this model using real data. It is planned to set up a physical network of sky cameras in the target region to collect real images and irradiance measurements. This realworld data set will be crucial to thoroughly evaluate the practical performance, robustness, and generalizability of the model. It will allow the necessary fine-tuning and adjustment to account for the inherent stochasticity and complexity of actual atmospheric conditions.

In addition to evaluating the forecasting accuracy, the practical feasibility of deploying a multi-camera system must also consider the cost of individual units. The proposed camera modules were designed using low-cost, off-the-shelf components with the goal of supporting scalable deployment. Table II summarizes the hardware components and their associated costs, with the total price of one complete unit remaining below C60. This cost-effective configuration, based on opensource platforms and simple solar power integration, makes the system suitable for distributed implementations in both research and real-world settings. The affordability and modularity of the setup support its application in community monitoring, smart grid demonstrations, and large-scale regional deployments.

TABLE II

COMPONENT COST BREAKDOWN FOR F SINGLE SKY CAMERA UNIT (2023).

Component	Description	Price [€]
Raspberry Pi Camera	Wide-angle camera compatible with Raspberry Pi	18.32
Raspberry Pi Zero W	Mini computer (single-board)	27.50
Small Solar Panel	5V, 0.125 W (45 × 25 mm)	1.59
INA219 Module	Current and voltage measurement module	7.30
3D-Printed Housing	Protective enclosure	0.89
Mounting Clamp	For camera mounting	1.31
Total		**56.91**

V. CONCLUSION

The growing adoption of photovoltaic (PV) systems in modern energy grids presents both opportunities and challenges, particularly with regard to the variability of solar energy production. Accurate short-term forecasting of solar irradiance plays a crucial role in ensuring stable and efficient grid operation. This paper demonstrates the potential of using a synthetic database in combination with a machine learning model to overcome these challenges by analyzing cloud dynamics using multiple sky cameras.

The synthetic database developed in this study provides a controlled environment for testing different model configurations, weather conditions, and data structures. This flexibility allows systematic experimentation with different parameters to analyze the potential for regional solar irradiance forecasting. By using images from multiple cameras strategically distributed across the monitored region, the model can detect patterns in cloud movement and shadow dynamics. The results show that the use of multiple cameras significantly improves forecasting accuracy compared to a single-camera setup.

The performance evaluation across the three defined scenarios confirms that multiple perspectives contribute to more accurate predictions, not only for locations with installed cameras but also for locations without direct visual input. The model has successfully demonstrated that it is able to predict solar irradiance at the central target location using only the data from the peripheral cameras. This finding highlights the potential of a distributed camera network to support regional solar forecasting without the need for a dense sensor installation.

The results show that using multiple cameras gives the model a more detailed understanding of cloud dynamics, which in turn improves forecast accuracy. By capturing cloud movement from different angles, the model gains insight into shadow behavior and irradiance variations. This capability is particularly useful for forecasting production at locations without direct camera measurements.

In addition, the synthetic database supports the simulation of camera placements in real regions, enabling the development of optimal configurations for specific locations. This approach makes it possible to train the model in a synthetic environment and then reconcile it with real data. As the synthetic database can be created much faster than collecting real data (in minutes rather than days) it provides a practical and efficient solution for testing different configurations. Once the model has been trained in this flexible environment, it captures the dependencies between cloud movement and shadow formation, reducing the amount of real data needed to fine-tune it to the actual meteorological conditions at the selected location.

Alen Jakoplić, Dubravko Franković, Tomislav Plavšić, Branka Dobraš, Regional Solar Irradiance Forecasting Using Multi-Camera Sky Imagery and Machine Learning Models, Journal of Energy, vol. 73 Number 4 (2024), 26–33
https://doi.org/10.37798/2024734707

This research underlines the importance of flexible, dataefficient approaches to renewable energy forecasting. The method presented not only demonstrates the feasibility of regional predictions of solar irradiance but also highlights the potential of multi-camera systems for accurate forecasting over larger areas. By enabling predictions on a regional scale, this work provides a solid foundation for future advances in solar energy forecasting and its practical implementation in power grid operations.

Future research will focus on deploying the camera modules in real-world environments and collecting observational data to validate the model's forecasting capabilities under actual atmospheric conditions. The ultimate goal is to enable reliable, region-wide solar irradiance forecasting based on a distributed network of low-cost sky imagers. The synthetic framework and results presented in this study provide a robust foundation for this transition and serve as a critical preparatory step toward real-world implementation.

References

[1] A. Qazi, F. Hussain,N.A. Rahim, G. Hardaker, D. Alghazzawi, K. Shaban, & K. Haruna, Towards sustainable energy: a systematic review of renewable energy sources, technologies, and public opinions, IEEE access, 7, 63837-63851, 2019.

[2] Murdock, Hannah E., et al., Renewables 2021-global status report, 2021.

[3] Kumar, Varun, A. S. Pandey, and S. K. Sinha., Grid integration and power quality issues of wind and solar energy system: A review, International conference on emerging trends in electrical electronics & sustainable energy systems (ICETEESES). IEEE, 2016.

[4] Impram, S., Nese, S. V., & Oral, B., Challenges of renewable energy penetration on power system flexibility: A survey, Energy Strategy Reviews, 31, 100539, 2020.

[5] Infield, D., & Freris, L., Renewable energy in power systems, John Wiley & Sons, 2020.

[6] Anvari, M. et al., Short term fluctuations of wind and solar power systems. New Journal of Physics 18, 063027, 2016., New Journal of Physics 18, 063027, 2016.

[7] Akhter, M. N., Mekhilef, S., Mokhlis, H., & Mohamed Shah, N., Review on forecasting of photovoltaic power generation based on machine learning and metaheuristic techniques, IET Renewable Power Generation, 13(7), 1009-1023, 2019.

[8] G. e. Boyle, Renewable electricity and the grid: The challenge of variability, London, UK: Earthscan Publications Ltd., 2012.

[9] S. Jenniches, Assessing the regional economic impacts of renewable energy sources – A literature review, Renewable and Sustainable Energy Reviews, Volume 93, Pages 35-51, ISSN 1364-0321, 2018.

[10] Chaturvedi, D. K., & Isha, I., Solar power forecasting: A review, International Journal of Computer Applications, 145(6), 28-50, 2016.

[11] Yang, B., Zhu, T., Cao, P., Guo, Z., Zeng, C., Li, D., ... & Yu, T., Classification and summarization of solar irradiance and power forecasting methods: A thorough review, CSEE Journal of Power and Energy Systems, 2021.

[12] U. &. W. Z. Munawar, A framework of using machine learning approaches for short-term solar power forecasting, Journal of Electrical Engineering & Technology, 15(2), 561-569, 2020.

[13] Wang, F., Mi, Z., Su, S. and Zhao, H., Short-term solar irradiance forecasting model based on artificial neural network using statistical feature parameters, Energies, 5(5), pp.1355-1370, 2012.

[14] Sivaneasan, B., Yu, C.Y. and Goh, K.P., Solar forecasting using ANN with fuzzy logic pre-processing, Energy procedia, 143, pp.727-732, 2017.

[15] Wentz, V.H., Maciel, J.N., Gimenez Ledesma, J.J. and Ando Junior, O.H., Solar Irradiance Forecasting to Short-Term PV Power: Accuracy Comparison of ANN and LSTM Models, Energies, 15(7), p.2457, 2022.

[16] Oh, M., Kim, C.K., Kim, B., Yun, C., Kang, Y.H. and Kim, H.G., Spatiotemporal optimization for short-term solar forecasting based on satellite imagery, Energies, 14(8), p.2216, 2021.

[17] Cheng, L., Zang, H., Wei, Z., Ding, T., Xu, R., & Sun, G., Short-term solar power prediction learning directly from satellite images with regions of interest, IEEE Transactions on Sustainable Energy, 13(1), 629-639, 2021.

[18] Miller, S.D., Rogers, M.A., Haynes, J.M., Sengupta, M. and Heidinger, A.K., Short-term solar irradiance forecasting via satellite/model coupling, Solar Energy, 168, pp.102-117, 2018.

[19] Ryu, A., Ito, M., Ishii, H., & Hayashi, Y., Preliminary analysis of short-term solar irradiance forecasting by using total-sky imager and convolutional neural network, 2019 IEEE PES GTD Grand International Conference and Exposition Asia, 2019.

[20] Feng, C., Zhang, J., Zhang, W., & Hodge, B. M., Convolutional neural networks for intra-hour solar forecasting based on sky image sequences, Applied Energy, 310, 118438, 2022.

[21] Ahmed, R., Sreeram, V., Mishra, Y., & Arif, M. D., A review and evaluation of the state-of-the-art in PV solar power forecasting: Techniques and optimization, Renewable and Sustainable Energy Reviews, 124, 109792, 2020.

[22] Kaggle dataset, "Multi-Camera Solar Forecasting Dataset" [Online]. Available: https://www.kaggle.com/datasets/alenjakopli/ multicamera-solar-forecasting-dataset. [Accessed: Feb. 2025].

ENERGIJA